ORIGINAL PAPER

Synoptic-dynamic analysis of precipitation anomalies over Iran in different phases of ENSO

Jalil Helali[1] · Hossein Momenzadeh[2] · Saadoun Salimi[3] · Seyed Asaad Hosseini[4] · Mohammad Lotfi[2] ·
Seyedeh Maryam Mohamadi[5] · Gholamreza Maghami Moghim[6] · Farshad Pazhoh[3] · Mohammad Ahmadi[7]

Abstract

The study of teleconnection patterns is important to define and predict the temperature and precipitation anomalies and climate changes on a regional scale. In this study, the precipitation anomalies and intensities are analyzed in different El Niño–Southern Oscillation (ENSO) phases based on statistic-synoptic and dynamic approaches in Iran's basins. For this purpose, a network of 717 meteorological stations and rain gauges was created during the period 1987–2015 in 6 basins and 30 sub-basins in Iran. The precipitation anomalies and intensities of these basins were statistically analyzed in different ENSO phases and Oceanic Niño Index (ONI), respectively. To analyze the synoptic and dynamic conditions in a medium El Niño, the negative and positive anomalies in the precipitation were examined in winter 2003 and spring 1992 using monthly European Centre for Medium-Range Weather Forecasts (ECMWF) data. Also, moisture flux convergence (MFC) was calculated and plotted for the lower (850–1000), middle (700–750), and upper (500–600) hPa troposphere layers using GrADS. The results of the precipitation anomalies showed positive and negative fluctuations of ± 100 to ± 150 mm in ENSO phases and ± 50 mm in the neutral phase. Consequently, the seasonal and annual precipitation anomalies were escalated in different ENSO intensities and their different phases. Moreover, it was found that the southeastern, eastern, and central plateau basins were slightly affected by the ENSO. Synoptic and dynamic analysis of precipitation anomalies also demonstrated the role of westward displacement (sea to land) and eastward (land to sea) components of Saudi Arabia's high-pressure system. During the positive precipitation anomalies (with a significant eastward displacement to the east and settled on the Arabian Sea), advection of heat and humidity toward Iran and penetration trough in the Middle East caused the increased intensity and extension of precipitations.

Keywords Iran · Precipitation anomaly · Basin · Synoptic and dynamic analysis · ENSO · MFC

Introduction

As one of the most important climatic and hydrological variables, precipitation has a significant environmental impact on the living system on the Earth. Therefore, precipitation prediction and its management play a crucial role in various sectors such as water resources and agriculture, especially in arid and semi-arid regions (e.g., Iran). Previous studies showed that the seasonal and annual precipitation trends of the major Iranian meteorological stations in a period of 50 years (1965 to 2005) experienced a decreasing trend between − 2 and − 4.3 mm per year (Tabari and Talaee Hosseinzadeh 2011), which was alarming for such area and population. Aside from that, the teleconnection indices were proven to be important factors affecting the climatic variables in precipitation (Kalimeris et al. 2017; Ahmadi et al. 2019; Helali et al. 2020; Dehghani et al. 2020; Helali et al. 2021a, b), extreme precipitation (Jiang et al. 2019; Atif et al. 2020), prediction of flow rate and runoff (Ghodousi and Kooshafar 2018; Nalley et al. 2019), yield of agricultural products (Araghi et al. 2019), drought, warm and dry periods (Mohammadrezaei et al. 2020), groundwater (Liesch and Wunsch 2019), climate changes (Ghasemi and Khalili 2008), and last spring frost and chilling (Sabziparvar et al. 2020; Helali et al. 2021a, b).

✉ Seyed Asaad Hosseini
  Hosseini.asad8@gmail.com

Extended author information available on the last page of the article

In this context, a number of regional studies regarding the Southern Oscillation extreme phase examined the hydro-meteorological variables in low and middle latitudes (Rasmusson and Wallace 1983; Ropelewski and Halpert 1986; Kahya and Dracup 1994; Price et al. 1998). According to their results, there were strong evidences of an intense relationship between the ENSO and precipitation patterns. Generally speaking, the precipitation is mainly affected by ENSO across the globe (Rasmusson 1984; Schmidt et al. 2001; Grimm et al. 1998; Kadioğlu et al. 1999; Gong and Wang 1999; Nazemosadat and Cordery 2000, 2004; Ahmadi Givi et al. 2010; Rahimi et al. 2016; Araghinezhad et al. 2016; Nicholson 2001; Pagano et al. 2003; Wang and Hendon 2007; Zanchettin et al. 2008; Monzon et al. 2012). Precisely, the abovementioned research demonstrated various effects of the ENSO phenomenon with different lag times on precipitation quantities. Therefore, the increase and decrease in precipitation in different phases depend on the geographical area, distance, and proximity to the ENSO indices. To the best of our knowledge, the main gaps among those studies were defined as neglecting the precipitation anomalies in the research in different phases of teleconnection indices as well as its different intensities in the basin scale. The main purposes of this study were to investigate the seasonal and annual precipitation anomalies in different ENSO phases and intensities on the scale of Iran's sub-basins (30 sub-basins) from the statistic, synoptic, and dynamic points of view. In addition, the relationship between large-scale circulation patterns and two sample years of negative and positive precipitation anomalies was explored to determine the corresponding synoptic and dynamic conditions which led to the different behaviors of precipitation during a medium El Niño in Iran. Considering the type of ENSO phases and intensities, the analysis and outcomes would practically improve regional and long-term decision-making on water resources management.

Data and methodology

The present study was conducted in Iran including six main basins: (1) Caspian Sea (CS) with 7 sub-basins, (2) the Persian Gulf-Oman Sea (PG) with 9 sub-basins, (3) Urmia Lake (UL) with one sub-basin, (4) Central Plateau (CP) with 9 sub-basins, (5) the Eastern Boundary (EB) with 3 sub-basins, and (6) Qara Qom (QQ) with one sub-basin. The geographic locations of the basins can be found in Fig. 1. Table 1 represents the characteristics of these basins. The datasets of 717 rain gauge stations during the climatic period 1988–2015 were provided by the Ministry of Energy and the Meteorological Organization. The synoptic dataset was downloaded from ECMWF (https://www.ecmwf.int/) and

the ENSO indices could be found in NCEP/NCAR (https://psl.noaa.gov/data/gridded/data.ncep.reanalysis.html).

Next, the total precipitation of autumn, winter, spring, and annual precipitation was calculated based on monthly data. To classify the intensity of the ENSO phenomenon, an Oceanic Niño Index (ONI) in the region of Nino 3.4 was used (5 northern degrees north and 5 southern degrees and 170–120° west). In general, three common phases are mostly used within the research community, namely warm phase, cold phase, and neural. The warm phase (El Niño) is defined as a time on which the average quarterly amount mean value of the ONI is more than 0.5 in 5 consecutive months, whereas the cold phase (La Niña) occurs when it is less than − 0.5; otherwise, the phase is considered as neutral. When ONI is between 0.5 and 0.9, 1.0, and 1.4, and more than 1.5, El Niño is considered as weak, medium, and strong, respectively. Furthermore, the weak, medium, and strong La Niña range between − 0.5 and − 0.9, − 1.0, and − 1.4, and less than − 1.5, respectively. Seasonal and annual precipitation anomalies were mapped in different ENSO phases and intensities using the ArcGIS software version 10.4. Then, the SAS software was used to investigate the significance or non-significance of precipitation anomalies in different ENSO phases and intensities based on the *T*-test. Dynamic and synoptic analysis; the datasets from 1994, 2009, and 2015 for the years of El Niño; and the datasets from 1995, 1998, 2007, and 2016 for La Niña were utilized. Moreover, high-level data including retrieved data of geopotential height, sea level pressure, zonal wind, meridian wind, specific humidity, and precipitation components were obtained from the ECMWF Data Center Ver. 5 (Dee et al. 2011) to investigate the synoptic condition of winter 2003 with negative precipitation anomaly and spring 1992 with positive precipitation anomaly during El Niño phase with medium intensity. The spatial resolution of the data was 0.25° ranging between 10–60° north and 10–80° east in which the atmospheric synoptic scale systems were well traceable. Exploiting the GrADS software, the monthly pressure average maps, wind vector of sea level, geo-potential height, wind vector of 500 hPa, moisture flux convergence (MFC), and precipitation anomaly were generated. In order to identify the fluctuation of the behavior of atmospheric synoptic scales, the anomalies of pressure and wind vector maps at sea level and height and wind vector at 500 hPa level were calculated and plotted, as well. In this study, the synoptic-teleconnection from a distance was considered as an effective approach (Ahmadi et al. 2019) to better explain the relationship between spatial–temporal atmospheric global circulation changes and Iran's precipitation. The MFC value was calculated and analyzed to identify the sources of humidity supply for super heavy precipitations. Based on the principle of water vapor continuity in the isobaric coordinate system, the MFC equation can be expressed as follows:
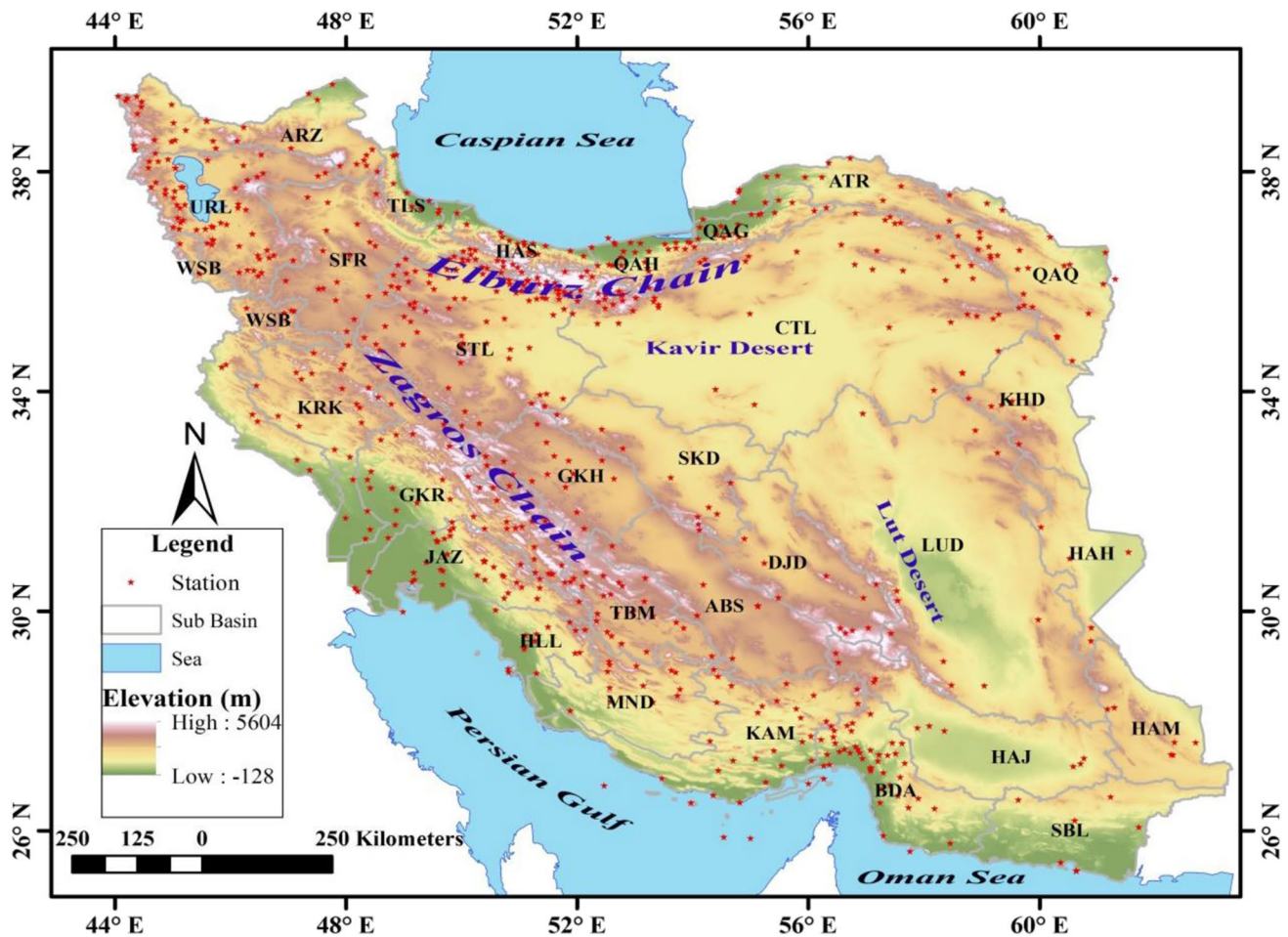
Fig. 1 Geographical distribution of rain gauge station study

$$MCF = -\nabla, (q\vec{V}_h) = -V_h, \nabla q - q\nabla, \vec{V}_h \tag{1}$$

$$MCF = -q\left(\frac{\partial u}{\partial x} = \frac{\partial v}{\partial y}\right) - u\frac{\partial q}{\partial x} - v\frac{\partial q}{\partial y} \tag{2}$$

where $-\nabla, (q\vec{V}_h)$ is the moisture convergence flux, $-\nabla, (q\vec{V}_h)$ is the humidity advection, $-\nabla, (q\vec{V}_h)$ is the moisture convergence, q is the specific humidity, x and y are independent spatial variables, and u and v are the zonal and meridian wind components. In this equation, the phrase "advection" means a horizontal advection of specific humidity. The phrase "convergence" expresses the product of the specific humidity in the convergence of flow volume (Banacos and Schultz 2005). In this study, the MFC was calculated and plotted for the lower (850–1000), middle (700–750), and upper (500–600) hPa troposphere layers during winter 2003 and spring 1992 (Darand and Pazhoh 2019a, b).

Results and discussion

Seasonal and annual spatial analysis

Figure 2 shows the analysis of seasonal and annual precipitation anomalies. Based on the obtained results, the major autumn precipitation anomaly of sub-basins in the El Niño phase was up to + 50 mm (in the western and southwestern parts were + 100 mm). In the weak El Niño in the western and southwestern sub-basins, these anomalies ranged from + 100 to + 150 mm (in the southeastern sub-basins are up to − 50 mm); in the medium El Niño in most sub-basins, anomalies were up to + 50 mm and in the southwestern sub-basins reached − 100 mm (in some sub-basins such as STL, CTL, QAG, ATR, and QRQ are up to − 50 mm). In the strong El Niño in major sub-basins, the precipitation anomaly reached + 50 mm, and in the PG basin ranged between 100 and 150 mm (precipitation anomaly

Table 1 Characteristics of the meteorological stations in Iran's basins

Main basin name	Main basin abbreviation	Sub-basin name	Sub-basin abbreviation	Area (M ha)	Number of stations	Average of autumn Pr. (mm)	Average of winter Pr. (mm)	Average of spring Pr. (mm)	Average of annual Pr. (mm)
Basin 1—Caspian Sea	B1-CS	Aras	ARZ	4.099	32	72	60.3	125.6	300
		Atrak	ATR	2.699	14	84.5	121.3	90.9	335.2
		Haraz-Sefidroud	HAS	1.1	14	452.8	246.3	164.7	1091.5
		Qarasu-Gorgan	QAG	1.325	19	151.9	165.7	123.4	521.2
		Qarasu-Haraz	QAH	1.884	30	234.9	178.8	120.9	659.3
		Sefidroud	SFR	5.961	34	144.4	138.6	137.8	457.7
		Talesh Rivers	TLS	0.696	8	496.6	278.4	184.4	1253.6
Basin 2—Persian Gulf and Oman Sea	B2-PG	Bandarabas-Sedij	BDA	4.068	45	38.7	130.6	20.1	201.1
		Great Karoun	GKR	43.6	44	157.8	257.9	100.0	517.4
		Helleh	HLL	1.98	13	109.9	189.0	35.8	336.6
		Jarahi-Zohreh	JAZ	3.842	36	138.7	219.3	59.8	419.4
		Kal-Mehran	KAM	5.757	30	37.2	112.2	26.6	191
		Karkheh	KRK	5.011	24	128	168.5	95.2	393.5
		Mand	MND	4.387	15	95.2	214.4	51.4	366.7
		South Balouchestan	SBL	4.379	7	32.8	73.1	19.8	141.4
		West Boundary	WSB	3.889	13	148.5	213.9	118.5	484
Basin 3—Urmia Lake	B3-UL	Urmia Lake	URL	5.272	58	96	99.7	116.3	325.6
Basin 4—Central Plateau	B4-CP	Abarkouh-Sirjan	ABS	5.357	7	38	90.9	37.1	168.3
		Central Desert	CTD	22.418	55	47.8	85.7	66.2	211.7
		Daranjir Desert	DJD	4.767	10	28	86.4	35.2	152.2
		Gav Khouni	GKH	3.988	18	91.3	142.8	75.5	312.1
		Hamoon-Jaz-morian	HAJ	6.352	11	21.1	84.1	24.1	144.8
		Lut Desert	LUD	19.499	11	18.5	71.1	27.9	118.6
		Siahkouh Desert	SKD	4.706	8	30.4	59.7	36.7	128.4
		Salt Lake	STL	9.135	92	98.9	123.1	107.0	341.2
		Tashk-Bakhtegan-Mahra	TBM	2.944	23	97.4	216.9	67.9	385.1
Basin 5—East Boundary	B5-EB	Hamoon-Hir-mand	HAH	3.189	5	11.6	53.6	16.6	82.3
		Hamoon-Mashkil	HAM	3.343	6	14.3	54.9	17.7	95.2
		Khuf Desert	KHD	3.208	6	32.2	103.1	41.6	177.4
Basin 6—Qara Qom	B6-QQ	Qara Qom	QRQ	4.421	29	45.6	105.1	88.4	243.7

Pr. precipitation

of −50 mm was observed in some sub-basins PG and CP). Analysis of autumn precipitation anomaly in the La Niña phase and its various intensities was mostly negative, so in the La Niña phase in most of the sub-basins, the precipitation anomaly of −50 mm (even −100 mm in some parts of WSB sub-basin) was observed, while precipitation anomaly of +50 mm occurred in some parts of CS, QQ, CP, and EB sun basins. In the weak and medium La Niña, the anomalies up to +50 mm were mainly seen in the majority of the basins, whereas the precipitation anomalies of −50 mm and even −100 mm (western and southwest parts) occurred in the strong La Niña. Based on the results, the autumn

precipitation anomaly in the neutral phase in most of the sub-basins was similar to La Niña phase anomalies, equal to − 50 mm. Accordingly, the autumn precipitation anomalies in the El Niño phases and intensities of + 50 to + 150 mm were observed, while in the La Niña phases and intensities and neural phase experienced − 50 mm (and even up to − 100 and − 150 mm) as shown in Fig. 2, column 1. Comparatively, our findings were in agreement with the results of Ghaedamini et al. (2014), Khorshiddoust and Ghavidel Rahimi (2006), and Nazemosadat and Ghasemi (2004). However, Ahmadi Givi et al. (2010) believed that Iran's precipitation was not affected by the ENSO phenomenon and its anomaly could not be analyzed by ENSO.

Analysis of winter precipitation anomaly also showed that in the El Niño and weak El Niño phases, the anomalies were up to + 50 mm (− 50 mm in the central plateau basin) in the mast of the sub-basins. In the medium El Niño in northern and southern parts, the anomalies rated + 50 and − 50 mm, respectively, and in the strong El Niño, it recorded + 50 mm (+ 100 mm in PG basin and − 50 mm in CP basin). Unlike the El Niño and its different intensities, the anomaly of winter precipitation in different La Niña phases and intensities did not follow a specific pattern. As a consequence, it was different in the La Niña and medium La Niña phases (mostly − 50 mm), in weak La Niña (− 50 to + 50 mm), and in strong La Niña (+ 50 mm; anomaly of + 150 mm in the northern part and − 50 to − 150 mm in the southern parts of Iran). In the neutral phase, the changes of winter precipitation anomalies were calculated by + 50 mm and − 50 mm in the southern and northwestern parts and the northern half of Iran, respectively. Therefore, winter precipitation anomalies were intensified at different intensities in terms of different ENSO phases, which was consistent with Hashemi Dovin (2013) and Mohammadi Sabet et al.'s (2017) outcomes (Fig. 2, column 2).

More analysis showed that the spring precipitation anomalies (in most of the sub-basins) varied from + 50 to − 50 mm, where spatially scattered in different phases and intensities of ENSO. In the El Niño phase with weak and medium intensities, an anomaly of + 50 mm (+ 100 mm in the northern half of Iran) was noticeable, but in the strong El Niño, a large part of the central and southeastern plateau and northwest part showed an anomaly of − 50 mm. The study of spring anomaly in different La Niña phases and intensities represented no specific pattern; however, it was mainly − 50 mm and intensified with increasing its intensity (in medium and severe La Niña − 100 mm in the northwest and + 50 mm in strong La Niña at the southeast). In the neutral phase, mostly positive anomalies were predominant in many parts of Iran (Fig. 2, column 3).

Investigation of annual precipitation anomalies in different El Niño phases and intensities reported the values up + 50 to + 150 mm, which was higher in the western, southwestern,

northern, and southeastern parts of Iran (in the central and southeastern parts in the medium and strong El Niño, the anomaly is − 50 mm). Nevertheless, different behaviors were observed in the La Niña phases and intensities. The results showed that the amount of anomaly in La Niña, medium La Niña, and strong La Niña varied between − 50 and less than − 150 mm (more severe anomaly in the west, northwest, and northeast). But in weak La Niña, the anomaly was − 50 to + 50 mm majorly in most parts of the country. Furthermore, in the neutral phase, a − 50 mm precipitation anomaly was predominantly observed in the region (except for some parts of the northwest with + 50 mm).

Our findings proved that the amount of annual precipitation anomalies in the El Niño and its different intensities was positive, while in the La Niña, medium La Niña, strong La Niña, and neutral phase, most areas and basins exhibited negative value. Figure 3 shows the relationship between precipitation and ENSO phases as a graphical model.

Statistical analysis of precipitation anomalies

Analysis of the significant seasonal and annual precipitation anomalies in different ENSO, La Niña, and El Niño phases are presented in Tables 2, 3, and 4, respectively. According to the results, the autumn precipitation anomaly was significant in the following phases and sub-basins: in the El Niño phase in SBL and SKD sub-basin (+ 16.4 and + 12.3 mm, respectively); in the La Niña phase in WSB, KRK, and LUD sub-basins (− 55.3, − 39.9, and − 4.5 mm, respectively); and in the neutral phase in the HAS, ATR, MND, LUD, CTD, DJD, KHD, and HAM sub-basins (52.3, − 13.6, − 27.3, − 6.2, − 14.1, − 9.8, − 11.8, and − 6.0 mm, respectively). Furthermore, the winter precipitation anomaly was insignificant in different ENSO phases, so the maximum anomalies were observed in the El Niño, La Niña, and neutral phases in the WSB, WSB, and GKH sub-basins, respectively (19.3, − 19.4, and 20.1 mm, respectively).

Precipitation anomalies of spring appeared as positive in El Niño and negative in La Niña phases (Table 2). The results analysis revealed that spring precipitation anomalies were significant in the El Niño phase in the ARZ, SFR, HAS, QAG, ATR, WSB, KRK, URL, STL, CTD, GKH, and QRQ sub-basins (22.6, 41.2, 20.8, 32.4, 30.5, 37.8, 31.3, 29.2, 39.3, 22.6, 15.5, and 29.3 mm) and in the La Niña phase in the ARZ, TLS, SFR, QAG, QAG, WSB, KRK, URL, STL, CTD, and QRQ sub-basins (− 31.4, − 31.9, − 39.4, − 30.9, − 32.3, − 42.1, − 28.7, − 40.3, − 34.9, − 24.7, and 36.7 mm), but in the neutral phase, the anomaly was mostly negative and non-significant.

Analysis of annual precipitation anomaly of Iran's sub-basins indicated positive and negative anomalies in the El Niño and La Niña phases, respectively; however, in the neutral phase, both types of anomalies were observed

Precipitation anomalies (mm)

< -150	-150 – -100	-100 – -50	-50 – 0	0 – 50	50 – 100	100 – 150	> 150
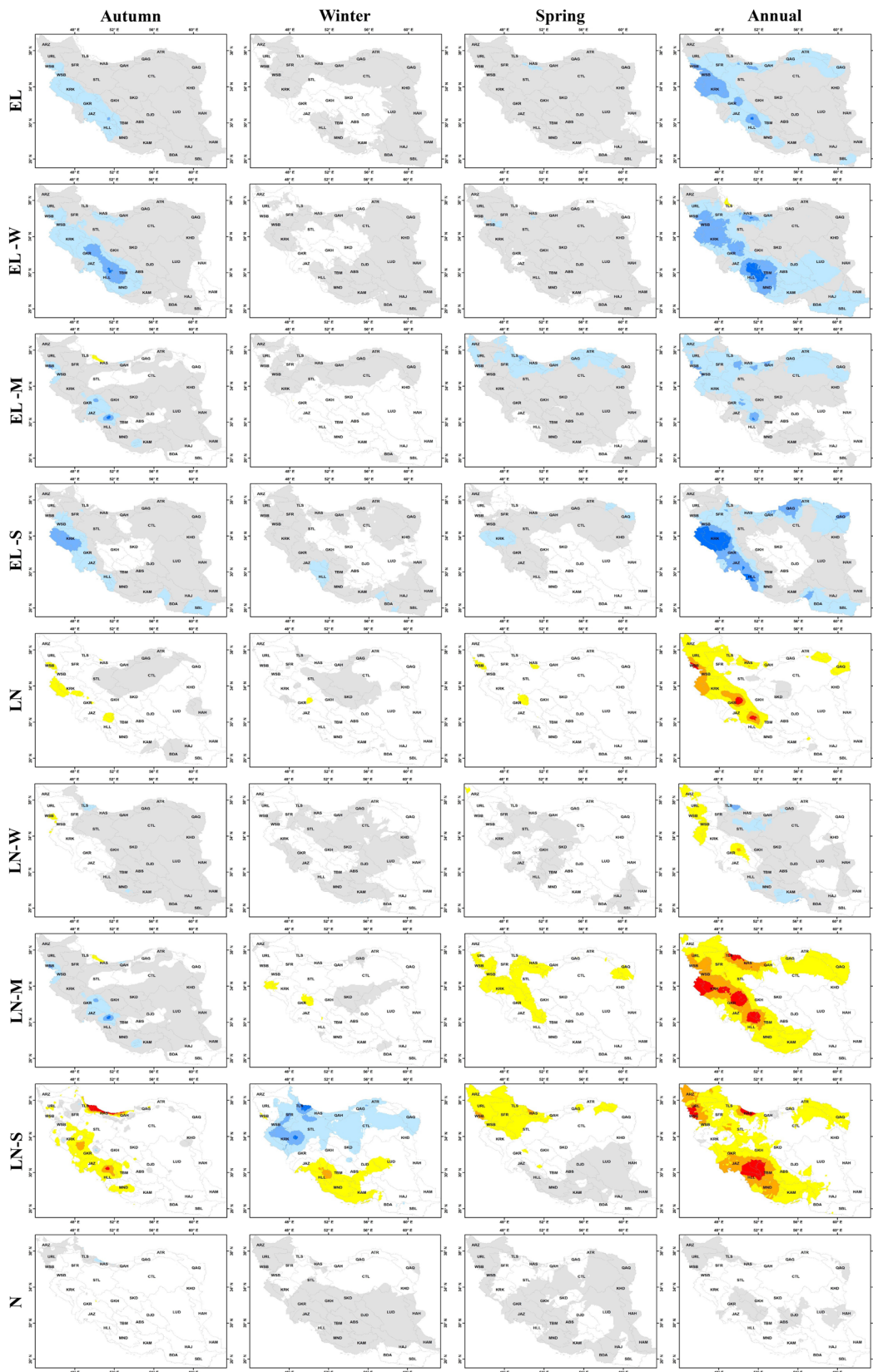
◀**Fig. 2** Seasonal and annual precipitation anomalies in different ENSO phases and intensities

(Table 2). Statistical analysis revealed that the annual precipitation anomaly of the El Niño phase in the sub-basins ARZ, SFR, ATR, WSB, KRK, URL, STL, CTD, and QRQ ($+36.0, +74.2, +52.6, +120.9, +99.1, +56.4, +66.7, +41.6,$ and $+52.5$ mm, respectively); in the La Niña phase in the sub-basins ARZ, SFR, ATR, WSB, KRK, URL, STL, and QRQ ($-51.8, -60.4, -25.6, -116.8, -78.3, -76.8, -42.9,$ and -52.7 mm, respectively); and in neutral phase in the ATR and URL (-27.0 and $+20.4$ mm, respectively) was significance (Table 2).

To summarize (Table 2), the maximum precipitation anomalies in the El Niño, La Niña, and neutral phases in the autumn were $+66.1, -55.3,$ and $+52.3$ mm respectively in the GKR, WSB, and HAS sub-basins; in winter, the maximum precipitation anomalies were $+17.9, +19.43,$ and $+20.13$ mm (in the sub-basins of QAH, WSB, and GKR, respectively); in the spring, the maximum precipitation anomalies were $+41.2, +42.1,$ and $+11.2$ mm (in SFR, WSB, and GKR sub-basins, respectively); and annual anomalies were $+120.9, -116.8,$ and -31.3 mm (in the WSB, WSB, and QAG sub-basins, respectively).

Analysis of precipitation anomalies at different intensities of the El Niño can be found in Table 3. As a result, the autumn precipitation anomaly in the weak El Niño was significant and fluctuated between -18.2 and to $+101.7$ mm in GKR, JAZ, HLL, MND, TBM, ABS, CTD, SKD, and DJD sub-basins with the values of $+97.1, +78.9, +82.6, +94.4, +101.8, +39.9, +29.9, +19.1,$ and $+28.9,$ respectively. In the medium El Niño, autumn precipitation anomalies changed between -30.2 and -63.6 mm, which were significant in the two sub-basins (KAM and SKD with the values of $+32.6$ and $+15.9$ mm, respectively). Finally, the autumn precipitation anomaly in strong El Niño was significant and altered between 14.5 and $+115.9$ mm in HAS, ATR, WSB, KRK, HLL, SBL, HAJ, LUD, KHD, HAH, HAM, and QRQ sub-basins ($+38.7, +31.6, +115.9, +98.3, +77.2, +90.7, +28.6, +21.4, +24.1, +18.5, +36.1,$ and $+20.3$ mm, respectively).

In addition, winter precipitation anomalies insignificantly varied between -23.9 and $+37.9, -29.8$ and $+15.9,$ and -17.9 and $+70.4$ mm, in weak, medium, and strong El Niño, respectively. Spring precipitation anomaly changed between -14.8 and $+37.8$ mm in weak El Niño, which was significant in SFR, HAS, WSB, URL, STL, and GKH sub-basins ($+37.8, +11.1, +31.2, +26.9, +27.7,$ and $+18.1$ mm, respectively). Meanwhile, the spring precipitation anomaly in medium El Niño fluctuated between -4.9 and $+81.9$ mm, which was significant in ARZ, TLS, SFR, HAS, QAH, QAG, ATR, WSB, URL, STL, CTD, GKH, and QRQ sub-basins ($+47.6, +81.9, +63.0, +35.1, +47.2, +66.3, +67.0, +50.5, +50.7, +61.1, +42.5, +17.3,$ and 48.6 mm, respectively).

Also, the spring precipitation anomaly in strong El Niño differed from -13.9 to $+53.4$ mm, which were significant in HAS, QAH, ATR, WSB, KRK, STL, CTD, and QRQ sub-basins.

The annual precipitation anomaly of weak El Niño varied between -144.4 and 133 mm, which were significant in SFR, WSB, KRK, URL, STL, TBM, LUD, CTD, SKD, GKH, WSB, URL, STL, TBM, LUD, SKD, and GKH ($+95.6, +97.4, +98.9, +71.8, +79.9, +133.0, +60.3, +39.3, +30.6, +68.9, +97.4, +98.9, +71.8, +79.9, +133, +60.3, +39.3, +30.6, +68.9,$ mm, respectively). In addition, in the medium El Niño, the annual precipitation anomaly fluctuated between -21.4 and $+102.6$ mm, significantly in ARZ, SFR, ATR, WSB, KRK, URL, STL, CTD, and QRQ sub-basins ($+62.5, +71.0, +71.5, +102.6, +50.6, +69.3, +72.1, +49.6, +55.3$ mm, respectively). Annual precipitation anomaly in strong El Niño changed between -12.7 and $+183.5$ mm and were significant in SFR, HAS, QAG, ATR, WSB, KRK, HLL, STL, CTD, and QRQ sub-basins ($+46.8, +110.3, +125.1, +91.3, +183.5, +172.1, +148.1, +38.8, +33.0, +91.2$ mm, respectively). Therefore, the annual and seasonal precipitation anomalies in different El Niño intensities intensified in comparison with those of El Niño phase (compare Tables 2 and 3).

Table 4 presents the analysis of seasonal and annual precipitation anomalies in different La Niña intensities. Autumn precipitation anomaly fluctuated between -53.6 and $+105.1$ mm in weak La Niña, which represented as significant in TLS, KAM, SBL, SKD, and WSB sub-basins ($+105.1, +31.9, +10.4, +12.9,$ and -53.6 mm, respectively). The values of autumn precipitation anomaly in the medium La Niña varied between -92.2 and $+19.2$ mm and were significant in WSB, KRK, MND, TBM, ABS, HAJ, LUD, DJD, KHD, HAM, and HAM ($-60.3, -50.7, -62.2, -47.3, -19.2, -13.6, -7.8, -14.6, -19.2, -13.6, -7.8, -14.6, -13.5, -5.7, -11.1$ mm, respectively). It was observed that the autumn precipitation anomaly in the strong La Niña changed between -197.4 and -2.0 mm which were significant in TLS, ATR, WSB, KRK, GKR, JAZ, HLL, MND, KAM, TBM, ABS, HAJ, LUD, SKD, DJD, HAH, and HAM sub-basins ($-131.6, -197.4, -22.5, -40.7, -51.3, -68.5, -83.1, -63.3, -57.8, -36.6, -58.5, -23.6, -16.8, -10.2, -29.5, -14.6, -10.5, -13.4,$ and 21.4 mm, respectively). The results showed that winter precipitation anomaly varied between -22.3 and $+17.9$ mm, -39.6 and $+6.9$ mm, and -84.6 and $+96.9$ mm in weak, medium, and strong La Niña, respectively, which were not statistically significant in any sub-basins (Table 4).

Spring precipitation anomaly in weak La Niña changes between -32.1 and $+11.7,$ so the values of an anomaly in ARZ, QAG, URL and QRQ sub-basins were significant ($-32.1, -15.1, -19.8,$ and -23.7 mm, respectively). In addition, the spring precipitation anomaly in medium La
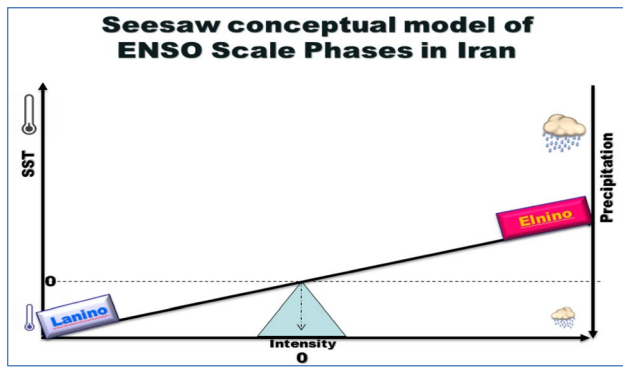
Fig. 3 Seesaw conceptual model of ENSO scale phases in Iran

Niña fluctuated between − 60.2 and − 3.1 mm and were mostly significant in ARZ, TLS, SFR, QAH, QAG, WSB, KRK, URL, STL, CTD, GKH, and QRQ sub-basins (− 2 3.0, − 32.4, − 59.3, − 43.5, − 42.9, − 60.2, − 46.9, − 47.6, − 59.9, − 39.4, − 40.3, and 45.3 mm, respectively). Finally, the value of spring precipitation anomaly in strong La Niña varied between − 83.1 and + + 21.6 mm, which were significant in ARZ, TLS, SFR, HAS, QAH, GAG, ATR, WSB, KRK, URL, STL, and CTD sub-basins (− 62.9, − 65.7, − 82.2, − 83.1, − 41.4, − 39.8, − 63.4, − 44.6, − 72.8, − 59.7, and − 37.3 mm, respectively). Hence, in different La Niña intensities, spring precipitation anomalies were negative and statistically significant in most of the sub-basins (Table 4).

The results showed that the annual precipitation anomaly in weak La Niña fluctuated between − 73.7 and + 33.4 mm

Table 2 Statistical significance of seasonal and annual precipitation anomalies in different phases of ENSO

Basin	Sub-basin	EL				LN				N			
		Autumn	Winter	Spring	Annual	Autumn	Winter	Spring	Annual	Autumn	Winter	Spring	Annual
CS	ARZ	10.7	2.87	22.6*	36.0*	− 9.9	− 5.1	− 31.4*	− 51.8*	− 0.6	2.3	8.9	15.8
	TLS	− 12.9	− 8.3	22.1	5.2	− 23.1	12.4	− 31.9*	− 43.0	36.0	− 4.3	9.9	37.6
	SFR	27.9	9.1	41.2*	74.2*	− 15.9	− 8.0	− 39.4*	− 60.3*	− 12.0	− 1.1	− 1.9	− 13.7
	HAS	− 8.4	6.3	20.8*	22.4	− 43.9	− 6.4	− 29.0	− 84.8	52.3*	0.1	8.2	62.6
	QAH	19.5	17.9	32.4*	62.7	− 8.3	− 3.8	− 30.9*	− 37.3	− 11.1	− 13.9	− 1.5	− 25.4
	QAG	14.5	7.9	35.5	55.8	5.6	2.5	− 32.3*	− 24.3	− 20.1	− 10.4	− 3.3	− 31.3
	ATR	14.9	8.4	30.3*	52.6*	− 1.2	0.1	− 27.7	− 25.6*	− 13.6*	− 8.4	− 2.7	− 27.0*
PG	WSB	64.4	19.3	37.8*	120.9*	− 55.3*	− 19.4	− 42.1*	− 116.8*	− 9.0	0.0	4.3	− 4.1
	KRK	57.9	10.1	31.3*	99.1*	− 39.9*	− 9.9	− 28.7*	− 78.3*	− 18.0	− 0.5	− 2.6	− 20.9
	GKR	66.1	− 1.4	22.3	86.6	− 45.1	− 15.2	− 33.5	− 94.0	− 21.1	16.7	11.2	7.3
	JAZ	62.9	4.4	13	79.8	− 42.9	− 14.9	− 19.0	− 76.7	− 19.9	10.6	6.0	− 3.2
	HLL	55.7	5.5	3.1	66.9	− 24.4	− 9.4	− 1.4	− 35.2	− 31.3	0.8	− 1.7	− 31.8
	MND	50.2	5.4	7	62.7	− 23.0	− 14.4	− 10.6	− 47.6	− 27.3*	9.1	3.7	− 15.1
	KAM	22.9	3.5	3.6	36	− 5.1	− 15.2	− 5.3	− 27.7	− 17.9	11.7	1.8	− 8.2
	SBL	16.4*	13.3	12	50.3	− 5.9	− 12.3	− 7.1	− 29.6	− 10.4	− 0.9	− 5.0	− 20.6
	BDA	21.3	7.2	− 0.8	33.2	0.2	− 7.4	− 2.1	− 12.5	− 21.6	0.2	2.9	− 20.7
UL	URL	28.3	0	29.2*	56.4*	− 28.4	− 8.0	− 40.3*	− 76.7*	0.1	8.0	11.1	20.4*
CP	STL	22.5	6.2	39.3*	66.7*	− 3.9	− 5.1	− 34.8*	− 42.9*	− 18.7	− 1.0	− 4.5	− 23.8
	TBM	44.3	1.1	13.3	58.8	− 22.2	− 15.1	− 16.5	− 53.9	− 22.1	13.9	3.1	− 4.8
	ABS	17.2	− 10.5	6.2	13.2	− 7.1	− 3.8	− 6.7	− 18.3	− 10.1	14.3	0.5	5.1
	HAJ	11.7	1.1	2.5	19.4	− 3.6	− 8.9	− 3.4	− 17.1	− 8.0	7.7	0.8	− 2.3
	LUD	10.7	5.3	6.3	22	− 4.5*	− 10.9	− 6.7	− 21.5	− 6.2*	5.7	0.4	− 0.4
	CTD	13.2	8.1	22.6*	41.6*	0.8	− 5.3	− 24.7*	− 26.7	− 14.1*	− 2.9	2.0	− 14.9
	SKD	12.3*	− 8.6	10.4	15.2	− 4.4	3.7	− 9.3	− 11.0	− 7.9	4.9	− 1.0	− 4.0
	DJD	15.2	− 3.3	9.9	22.1	− 5.5	− 6.9	− 7.4	− 20.2	− 9.7*	10.3	− 2.4	− 1.9
	GKH	32.8	− 5.2	15.5*	42.6	− 13.7	− 14.9	− 24.3	− 53.3	− 19.1	20.1	8.7	10.6
EB	KHD	16.9	3.2	8.5	28.2	− 5.0	− 0.5	− 17.9	− 22.9	− 11.8*	− 2.6	9.5	− 5.2
	HAH	4.8	3	− 0.5	7.9	− 0.3	− 8.6	− 2.1	− 11.4	− 4.5	5.6	2.7	3.4
	HAM	8.8	3.1	− 0.4	18.2	− 2.8	− 5.3	− 2.8	− 13.1	− 6.0*	2.1	3.2	− 5.0
QQ	QRQ	8.1	14.3	29.3*	52.5*	− 2.4	− 12.5	− 36.7*	− 52.7*	− 5.6	− 1.7	7.5	0.2

EL, El Niño; *LN*, La Niña; *N*, neutral

*Significant at $\alpha = 5\%$

Table 3 Statistical significance of seasonal and annual precipitation in different severities of El Niño

Basin	Sub-basin	EL-W				EL-M				EL-S			
		Autumn	Winter	Spring	Annual	Autumn	Winter	Spring	Annual	Autumn	Winter	Spring	Annual
CS	ARZ	13.7	− 1.9	11.2	28.5	6.4	8.8	47.6*	62.5*	12.5	1.2	2.1	7.4
	TLS	− 11.1	− 23.9	− 14.8	− 144.4	− 19.4	− 5.2	81.9*	71.9	− 5.8	10.5	− 12.5	129.5
	SFR	55.1	5.7	37.8*	95.6*	9.1	6.9	63.0*	71.0*	15.2	17.5	13.8	46.8*
	HAS	− 18.2	− 7.5	11.1*	− 45.2	− 30.2	4.2	35.1*	31.5	38.7*	30.2	13.8*	110.3*
	QAH	19.7	22.9	14.4	44.1	23.9	15.9	47.2*	67.1	12.6	13.1	37.2*	84.1
	QAG	26.5	− 0.3	2.4	1.6	− 8.6	17.4	66.3*	63.7	31.3	10.7	39.1	125.1*
	ATR	19.6	− 3.6	− 5.8	8.0	− 0.9	15.2	67.0*	71.5*	31.6*	16.2	29.6*	91.3*
PG	WSB	49.2	15.3	31.2*	97.4*	45.2	9.1	50.5*	102.6*	115.9*	40.6	28.6*	183.5*
	KRK	73.3	5.5	20.9	98.9*	15.5	9.1	26.9	50.6*	98.3*	19.8	53.4*	172.1*
	GKR	97.1*	− 6.5	12.9	102.7	62.1	− 22.0	28.4	68.2	25.8	36.9	27.3	90.1
	JAZ	78.9*	7.1	11.1	95.7	63.1	− 26.6	4.7	40.4	38.4	46.8	28.4	115.1
	HLL	82.6*	5.5	14.4	101.1	14.5	− 29.8	− 4.9	− 21.4	77.2*	70.4	− 1.8	148.1*
	MND	94.8*	22.9	8.6	126.8	16.1	− 17.9	12.0	8.6	34.5	14.2	− 2.7	47.7
	KAM	19.3	20.7	2.9	59.8	32.6*	− 23.2	12.9	19.1	13.8	17.9	− 9.4	25.7
	SBL	− 1.1	18.7	24.7	65.1	− 15.5	− 8.8	16.6	1.2	90.7*	38.2	− 13.8	101.8
	BDA	6.0	12.3	0.5	34.6	20.0	− 19.4	2.7	1.0	46.3	39.4	− 7.9	79.3
UL	URL	46.9	− 5.2	26.9*	71.8*	23.2	0.6	50.7*	69.3*	8.1	7.2	0.5	13.8
CP	STL	45.6	2.0	27.7*	79.9*	6.5	12.7	61.1*	72.1*	11.9	2.8	24.1*	38.8*
	TBM	101.8*	8.5	23.7	133.0*	18.6	− 19.9	15.9	14.0	− 3.5	21.5	− 6.1	14.5
	ABS	39.9*	7.1	18.1	64.7	7.9	− 23.2	7.8	− 7.1	− 2.8	− 17.9	− 13.9	− 33.2
	HAJ	2.8	20.5	9.0	38.9	9.3	− 17.4	6.7	− 0.8	28.6*	− 0.1	− 13.3	20.3
	LUD	8.3	37.9	14.5	60.3*	5.9	− 22.4	7.8	− 9.1	21.4*	− 2.2	− 8.2	10.9
	CTD	29.9*	4.5	8.0	39.3*	2.1	9.9	42.5*	49.6*	4.8	10.7	14.7*	33.0*
	SKD	19.1*	− 10.0	20.8	30.6*	15.9*	− 12.2	14.5	18.2	− 3.4	− 0.9	− 11.4	− 12.5
	DJD	28.9*	19.7	15.5	64.1	4.1	− 20.2	18.0	3.2	11.4	− 12.6	− 10.8	− 12.7
	GKH	56.9	− 5.9	18.1*	68.9*	40.3	− 13.2	17.3*	42.7	− 14.5	7.6	9.0	2.9
EB	KHD	16.6	16.6	3.3	36.1	12.4	− 9.8	16.8	18.9	24.1*	2.5	3.9	30.2
	HAH	− 4.2	32.2	6.2	36.3	4.8	− 24.5	0.2	− 19.9	18.5*	0.7	− 11.7	7.2
	HAM	− 4.4*	17.1	5.9	43.3	3.8	− 16.9	1.2	− 13.8	36.1*	12.0	− 12.6	28.7
QQ	QRQ	11.5	13.7	− 3.1	23.9	− 3.5	11.7	48.6*	55.3*	20.3*	18.9	48.7*	91.2*

EL-W, weak El Niño; *EL-M*, medium El Niño; *EL-S*, strong El Niño

*Significant at $\alpha = 5\%$

and was significant in SFR, STL, ARZ, WSB, URL, and QRQ sub-basins (+ 12.9, + 33.4, − 44.8, + 7.4, − 73.7, − 43.6, and − 33.3 mm, respectively). In the medium La Niña, the annual precipitation anomaly varied between − 158.9 and − 18.8 mm and was significant in WSB, KRK, URL, STL, CTD, GKH, and QRQ sub-basins (− 47.1, − 111.9, − 61.3, − 34.2, − 158.9, − 123.6, − 92.6, − 95.3, − 52.7, − 81.7, and − 63.7 mm, respectively). The amount of annual precipitation anomalies in strong La Niña showed fluctuations between − 256 and − 23.1 mm which were significant in ATR, SFR, HAS, ATR, SWB, KRK, HLL, URL, STL, TBM, LUD, CTD, SKD, and QRQ sub-basins (− 91.3, − 74.3, − 256, − 45.9, − 77.7, − 61.8, − 127.5, − 112.9, − 61.8, − 140.0, − 38.8, − 50.1, − 56.9, and − 66.7 mm, respectively). In a nutshell, annual seasonal precipitation anomalies in different

La Niña intensities were intensified to compare with the La Niña phase (comparing Tables 2, 3, and 4).

To evaluate the effect of different ENSO phases and intensities on the seasonal and annual precipitation anomalies of the basins, the frequency of basins with significant anomalies was investigated. The results showed that the autumn precipitation anomaly in the El Niño, La Niña, and neutral phases was significant in 2, 3, and 8 sub-basins, respectively, whereas in the weak, medium, and strong El Niño, the autumn precipitation anomaly increased in 9, 2, and 12 sub-basins and in weak, medium, and strong La Niña increase in 5, 11, and 19 sub-basins (see Fig. 4 of the above image in the left side), respectively. Evaluation of the results in winter also revealed that the number of sub-basins with significant precipitation anomalies was not affected by

Table 4 Statistical significance of seasonal and annual precipitation in different severities of La Niña

Basin	Sub-basin	LN-W				LN-M				LN-S			
		Autumn	Winter	Spring	Annual	Autumn	Winter	Spring	Annual	Autumn	Winter	Spring	Annual
CS	ARZ	− 5.7	− 7.4	− 32.1*	− 44.8*	− 11.4	− 2.5	− 23.0*	− 47.1*	− 17.2	− 8.3	− 62.9*	− 91.3*
	TLS	105.1*	4.4	− 20.1	115.0	− 92.2	− 2.6	− 32.4*	− 152.4	− 131.6*	96.9	− 65.7*	− 78.1
	SFR	5.2	− 0.9	1.5	12.9*	− 28.0	− 23.9	− 59.3*	− 111.9*	− 30.9	34.1	− 82.2*	− 74.3*
	HAS	6.9	1.4	− 7.5	39.8	− 43.7	− 18.2	− 31.6	− 135.6	− 197.4*	17.2	− 83.1*	− 256.0*
	QAH	27.3	− 2.3	− 10.7	19.2	− 23.4	− 10.4	− 43.5*	− 81.7	− 55.2	17.8	− 41.4*	− 29.5
	QAG	31.0	0.0	− 15.1*	28.9	− 9.1	1.6	− 42.9*	− 61.3*	− 12.3	13.9	− 41.9*	− 35.9
	ATR	5.4	− 0.6	− 12.5	− 7.37*	− 0.8	− 3.7	− 36.1	− 34.2*	− 22.5*	17.5	− 39.8*	− 45.9*
PG	WSB	− 53.6*	− 8.8	− 10.8	− 73.7*	− 60.3*	− 39.6	− 60.2*	− 158.9*	− 40.7*	29.2	− 63.4*	− 77.7*
	KRK	− 21.7	− 1.8	1.1	− 23.3	− 50.7*	− 27.4	− 46.9*	− 123.6*	− 51.3*	35.8	− 44.6*	− 61.8*
	GKR	− 24.1	− 6.1	− 1.9	− 32.9	− 55.0	− 21.9	− 57.2	− 133.6	− 68.5*	− 15.7	− 33.2	− 118.9
	JAZ	− 21.5	1.0	2.8	− 17.7	− 48.9	− 16.4	− 38.9	− 103.6	− 83.1*	− 57.0	− 4.8	− 145.9*
	HLL	15.3	9.2	11.7	36.5	− 44.4	− 4.5	− 16.9	− 66.0	− 63.3*	− 84.6	21.6	− 127.5*
	MND	40.9	6.8	− 4.5	42.7	− 62.2*	− 13.1	− 21.8	− 95.0	− 57.8*	− 83.9	15.6	− 129.1
	KAM	31.9*	11.6	− 1.9	37.3	− 24.9	− 26.8	− 10.9	− 63.3	− 36.6*	− 48.7	6.5	− 80.6
	SBL	10.4*	− 22.3	− 1.6	− 24.1	− 11.9	− 1.4	− 9.8	− 23.7	− 30.4	− 26.1	− 12.6	− 69.9
	BDA	32.3	17.9	− 1.6	44.9	− 17.4	− 17.2	− 7.1	− 44.1	− 25.7	− 44.4	16.3	− 57.8
UL	URL	− 24.0	− 1.3	− 19.8*	− 43.6*	− 33.3	− 11.7	− 47.6*	− 92.6*	− 21.8	− 13.6	− 72.8*	− 112.9*
CP	STL	17.3	2.7	6.8	33.4*	− 14.6	− 20.5	− 59.9*	− 95.3*	− 23.8	32.8	− 59.7*	− 61.8*
	TBM	23.5	− 3.3	5.3	24.5	− 47.3*	− 14.3	− 30.5	− 91.2	− 58.8*	− 53.4	− 25.7	− 140.0*
	ABS	14.5	2.1	− 3.6	11.8	− 19.2*	− 4.1	− 11.1	− 34.5	− 23.6*	− 20.4	1.7	− 44.1
	HAJ	14.1	− 2.9	− 3.1	2.2	− 13.6*	− 7.4	− 7.9	− 26.9	− 16.8*	− 32.7	13.7	− 35.8
	LUD	1.9	− 2.7	− 7.9	− 9.1	− 7.8*	− 10.9	− 9.5	− 26.5	− 10.2*	− 35.6	7.9	− 38.8*
	CTD	11.5	− 0.4	− 0.8	15.8	− 4.7	− 11.2	− 39.4*	− 52.7*	− 8.9	3.9	− 37.3*	− 50.1*
	SKD	12.9*	4.4	0.8	17.6	− 11.1	6.9	− 15.6	− 21.0	− 29.5*	− 11.3	− 14.4	− 56.9*
	DJD	9.6	2.3	− 11.0	− 1.1	− 14.6*	− 8.4	− 11.6	− 33.4	− 14.6*	− 28.3	20.1	− 24.9
	GKH	− 7.4	− 6.8	− 4.1	− 17.8	− 18.9	− 21.7	− 40.3*	− 81.7*	− 11.7	− 11.7	− 20.4	− 46.1
EB	KHD	5.2	12.2	− 10.9	8.5	− 13.5*	− 5.6	− 25.7	− 45.1	− 2.0	− 17.8	− 8.0	− 28.2
	HAH	10.2	− 2.0	3.7	11.4	− 5.7*	− 8.2	− 7.0	− 21.1	− 10.5*	− 30.3	0.1	− 41.2
	HAM	11.8	− 1.1	− 5.2	− 2.2	− 11.1*	− 6.2	− 3.1	− 18.8	− 13.4*	− 14.2	5.7	− 23.1
QQ	QRQ	7.4	− 15.8	− 23.7*	− 33.3*	− 5.0	− 13.0	− 45.3*	− 63.7*	− 21.4*	− 0.6	− 41.6*	− 66.7*

LN-W, weak La Niña; *LN-M*, medium La Niña; *LN-S*, strong La Niña

*Significant at $\alpha = 5\%$

the different ENSO phases and intensities (see Fig. 4 of the above image on the right side). The number of spring precipitation anomaly in El Niño, La Niña, and neutral phases was significant at 12, 11, and 0 sub-basins, respectively. However, the precipitation anomaly increased in weak, medium, and strong El Niño in 6, 13, and 8, respectively, while in weak, medium, and strong La Niña, the precipitation anomaly increased to 4, 11, and 13 sub-basins (see Fig. 4 in the below image in the left side). On the other hand, the annual precipitation anomaly in the El Niño, La Niña, and Neutral was significant in 9, 8, and 2 sub-basins, respectively, while it was significant in the weak, medium, and strong El Niño in 10, 9, and 10 sub-basins, respectively. In weak, medium, and strong La Niña, it increased in 7, 11, and 15 sub-basins (see Fig. 4, below the image on the right side). Therefore,

the number of sub-basins with significant annual and seasonal precipitation anomalies at different ENSO intensities increased in comparison with its different phases (except for winter).

Therefore, it was found that there was a precipitation anomaly in different phases of ENSO that was in good agreement with similar studies conducted in different regions all around the world including Iran (e.g., Nazemosadat and Cordery 2000; Grimm et al. 1998; Nazemosadat and Ghasemi 2004; Zanchettin et al. 2008; Araghinezhad et al. 2016; Dehghani et al. 2020; Helali et al. 2021a, b) and differs from others (e.g., Gong and Wang 1999; Nicholson 2001; Ahmadi Givi et al. 2010; Monzon et al. 2012). The study conducted by Nazemosadat and Cordery (2000) explained significant autumn precipitation in the western parts of the Caspian
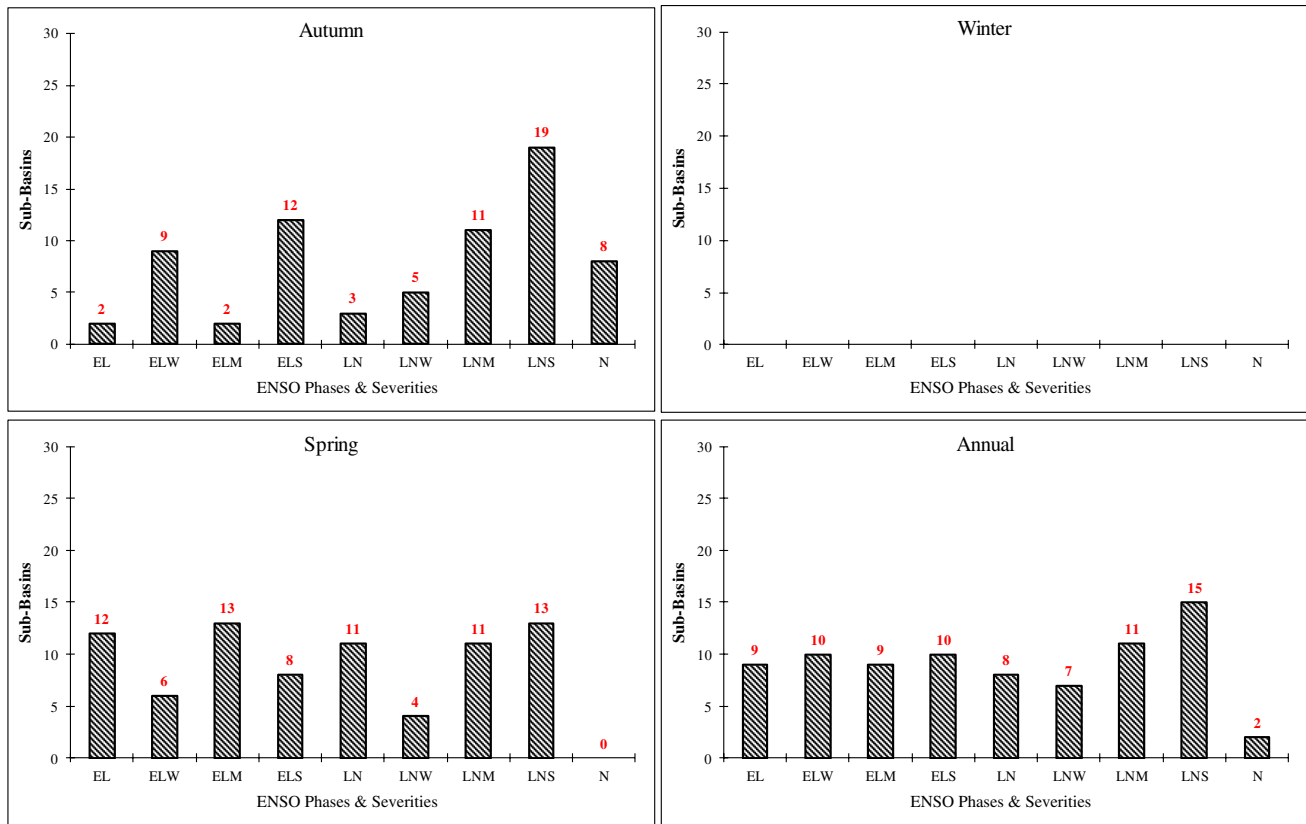
Fig. 4 The number of sub-basins with significant precipitation anomalies in different ENSO intensities and phases

Sea; however, our study showed that autumn precipitation anomaly in 2 sub-basins of SBL and SKD (in El Niño); sub-basins of WSB, KRK, and LUD (La Niña phase); and HAS, ATR, MND, LUD, CTD, DJD, KHD, and QRQ sub-basins (in the neutral phase) exhibited significant anomalies. The results of this study indicated the absence of significant winter anomalies in different ENSO phases and intensities, while Schmidt et al. (2001) studied the effect of winter precipitation in Florida on ENSO which was different from the results of the present study. The lack of significant precipitation anomaly in winter could attribute to the effect of other teleconnection indices, including the Black Sea and the Mediterranean SLP (Ghasemi and Khalili 2008).

The synoptic forcing simulation of the ENSO event in the Middle East and the introduction of the Sudan-Zagros convergence zone (RZCZ)

After statistical analysis, the reasons for the formation of suitable precipitation patterns in El Niño phases were briefly discussed. Using reanalysis of the pressure anomaly maps, geopotential height, and the NOAA center jets in three case extremes of El Niño (1982, 1997, and 2015) and three case extremes of La Niña on (1988, 1998, and 2010) on 40 years

ago, a model was simplified and a mean of atmospheric current in the Middle East was designed (Fig. 5). The outcomes of these maps showed that the sub-tropical jet (STJ) was usually stronger and more southern during the El Niño than the La Niña phase. In the El Niño phase, the convergence zone of the Red Sea usually strengthened and extended to Iran's plateau and the Zagros mountain range. This event, which is also visible in satellite images, is independent of Mediterranean cyclones, causing heavy and extensive precipitations, especially in Iran, Iraq, Kuwait, and Saudi Arabia. In the initial modeling, a simplified picture of the effect of El Niño and La Niña phases was provided, and a graphical prediction of the formation of a complex convergence zone was presented, which should be evaluated in an independent research. The mentioned convergence zone in this study is named Red Sea-Zagros (RZCZ) convergence zone or the Red Sea-Zagros (RZFZ) frontal zone. The mechanism of this convergence is such a way that with penetration of Mediterranean troughs and the establishment of cold and dry or cold and relatively humid currents by the Mediterranean and the Anatolian Plateau and the formation of the low-pressure Red-Mediterranean Sea, warm and mostly humid currents from the North Indian Ocean and its subsets to the low-pressure center which it has grown from the Red Sea to the
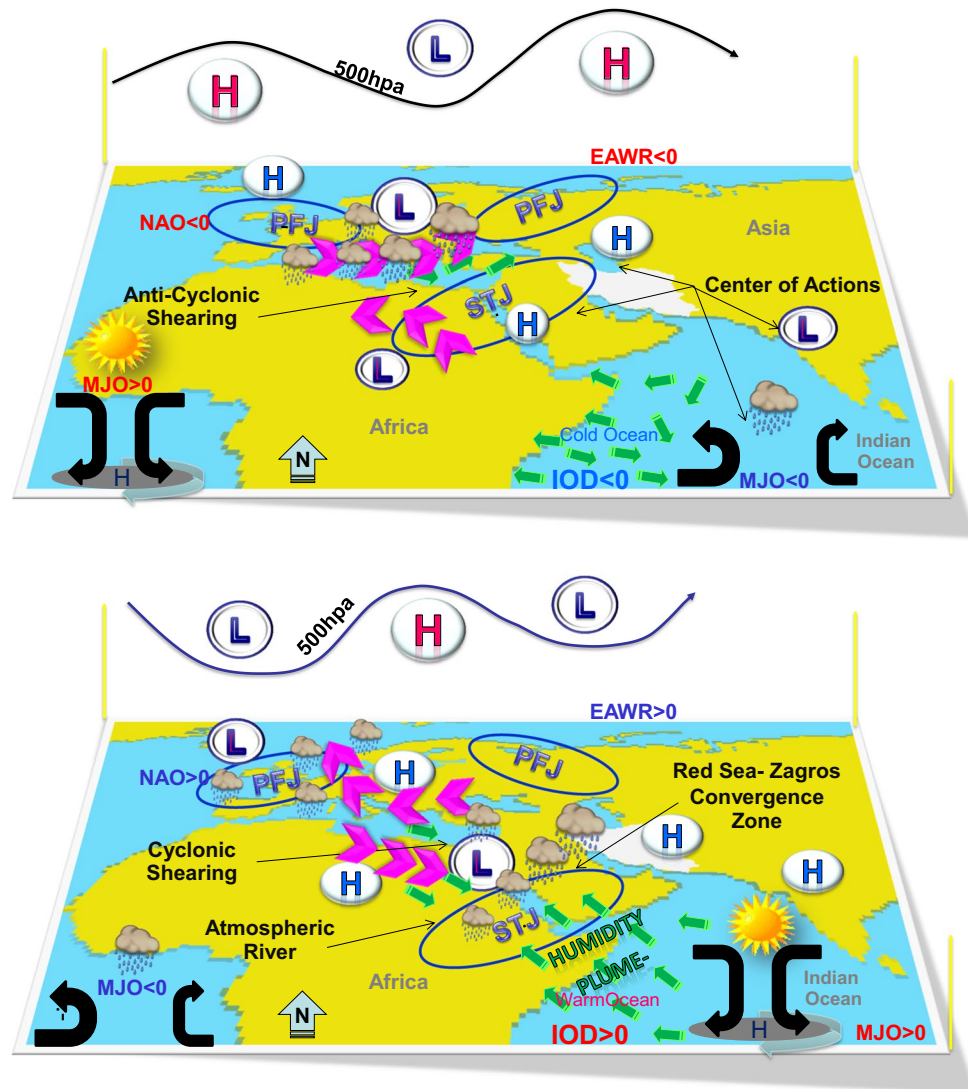
Zagros mountains penetrate and form a middle day semi-frontal zone. In the El Niño phase, the frequency of this convergence is significantly higher than that of La Niña. This unique convergence zone is the result of the interaction of the prevailing western winds and the systems of the tropical zones in the cold season. During the El Niño domination, on the Indian peninsula and the northeastern Indian Ocean, a positive pressure abnormality usually strengthens the eastern currents to strengthen at 850 hPa on the north of the Indian Ocean and toward the Red Sea. This suitable synoptic condition with penetration of deeper troughs of the eastern Mediterranean trough sometimes provides the mechanism of formation of atmospheric rivers (ARs) in RZCZ, including autumn 1994, autumn 2015, and spring 2019. In the La Niña phase, these suitable synoptic conditions usually weaken. El Niño phases are usually associated with the positive phase of the North Atlantic Oscillation; it seems that this coherence increased in the last decade. In El Niño phases, high pressures are usually amplified on Central and West of Europe, and North Africa, causing more cold and cyclone genesis airflow of eastern Mediterranean and the Red Sea (compatibility with the positive phase of NAO (North Atlantic Oscillation)). Usually, in the El Niño and La Niña phases, Indian Ocean Dipole (IOD) is in the positive and negative phases, respectively. The Madden–Julian Oscillation in the El Niño in west of Africa is also usually negative, which strengthens the convergence, but in La Niña causes the suppression and divergence. Strengthening the convergence in West Africa through expansion of the Hadley system will lead to the development of the induction trough in its northeast (the Mediterranean east trough). Air subsidence in the eastern 70° zone on the Indian Ocean bed has intensified in the El Niño phases as the Madden–Julian Oscillation has been positive, causing a suitable moisture flux-especially by considering to positive of IOD- toward Aden Gulf, Red Sea, and RZCZ area (Fig. 5).

Synoptic conditions led to negative anomalies of winter precipitation in 2003 and positive anomaly in spring 1992 in Iran during the medium phase

In the winter of 2003 and spring of 1992, El Niño was in a medium phase, but the precipitation anomaly was negative in winter and positive in spring in Iran. Therefore, in this section, the synoptic mechanism of the asymmetric effects of a medium El Niño on the precipitation situation of Iran is investigated.

Winter 2003

According to the pressure map and wind vector at the sea level (Fig. 6a) during winter 2003, the Siberian high pressure with a closed center of 1032 hPa is located in the north of Lake Balkhash that the resulting tongue, with zonal and meridian extensions, covers most of the study area and the country of Iran. With penetrating this cold high pressure, the contour tongue less than 1014 hPa corresponding to low-pressure systems has receded below 20° north latitude. With spreading this high pressure on Iran, surface divergent currents have been created, which has prevented the transfer of warm and humid air masses from the water resources of the Arabian and Red Seas (from the south) and the Mediterranean Sea (from the west) to Iran, causing the atmosphere stability.

The geopotential height and wind vector of 500 hPa (Fig. 6b) in winter 2003 indicate obviously the role of the huge height ridge (on the Atlantic Ocean) and high pressure of Saudi Arabia (in the south of the Red Sea and East of Africa) in creating a stable and non-turbulent atmosphere on the region. In addition to strong zonal advection at the 500 hPa level, the gradient of geopotential height in Iran increased, leading to barotropic conditions. The settlement of the Arabian high-pressure independent core strengthens the anticyclone movement of the atmosphere at middle levels of the troposphere which causes the convergence.

Figure 7 shows the MFC maps in g/kg/m/s in the lower layers (1000–850 hPa), the middle (750–700 hPa), and the upper (500–600 hPa) troposphere. Due to the settlement of high-pressure tongues on the sea level and the stability of the atmosphere in the middle levels of the troposphere, the MFC values are very small in Iran, and the lower layer of the troposphere (Fig. 7a) is less than 1.5 g/kg/m/s. Most of Iran, especially in the half western, lacks any MFC. Anticyclonic circulations on the Arabian Peninsula and Iran have prevented the transfer of MFC from adjacent water sources into the study region. In the middle and upper layers of the troposphere, with more reduction of MFC, caused the most part of the country had no humidity and only small spots corresponding to the Zagros Mountains in the half western of Iran have an MFC less than 0.75 g/kg/m/s. Usual conditions in the winter are the presence of deep troughs and synoptic-scale systems with high humidity. However, in winter 2003, as one of the dry seasons during the statistical period, the MFC rate was lower than normal and confirmed the drought conditions within the studied season.

Comparison of analysis of pressure anomaly and wind vector at the sea level in winter 2003 (Fig. 8a) with the 30-year mean value (1981–2010) showed the lack of penetration of cyclonic currents on the Mediterranean, Red Sea, and the Aden Gulf toward Iran and consequently cutting off
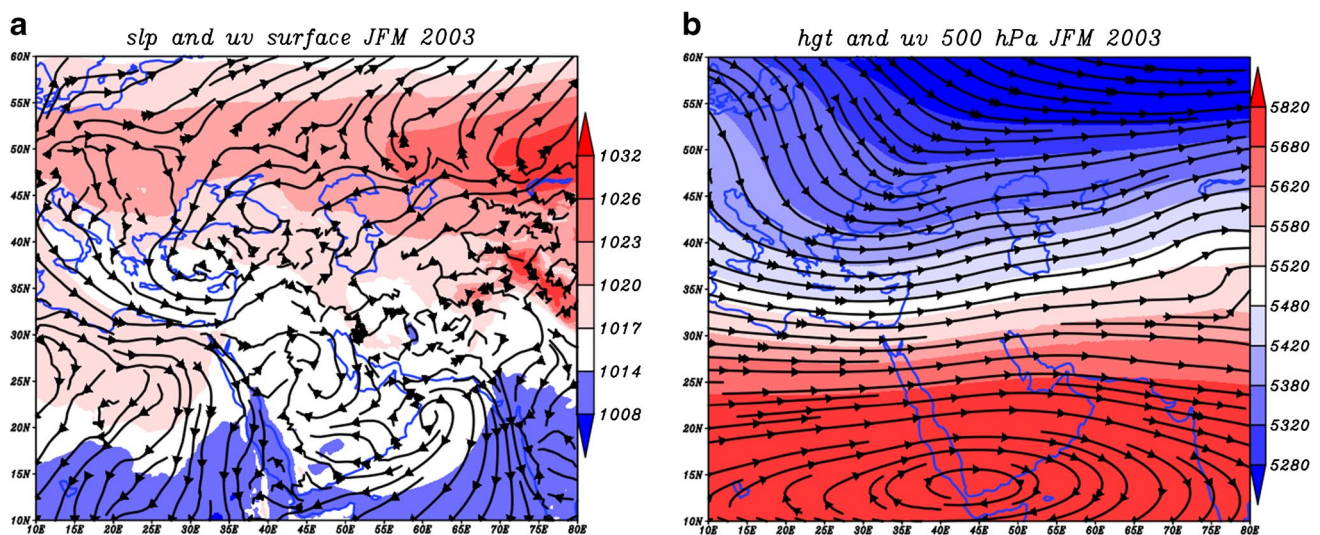

Fig. 6 **a** Pressure field (color) and surface wind currents (contour) at sea level in winter 2003 (January to March). **b** Geopotential height (color) and upper wind currents at 500 hPa in winter 2003 (January to March)
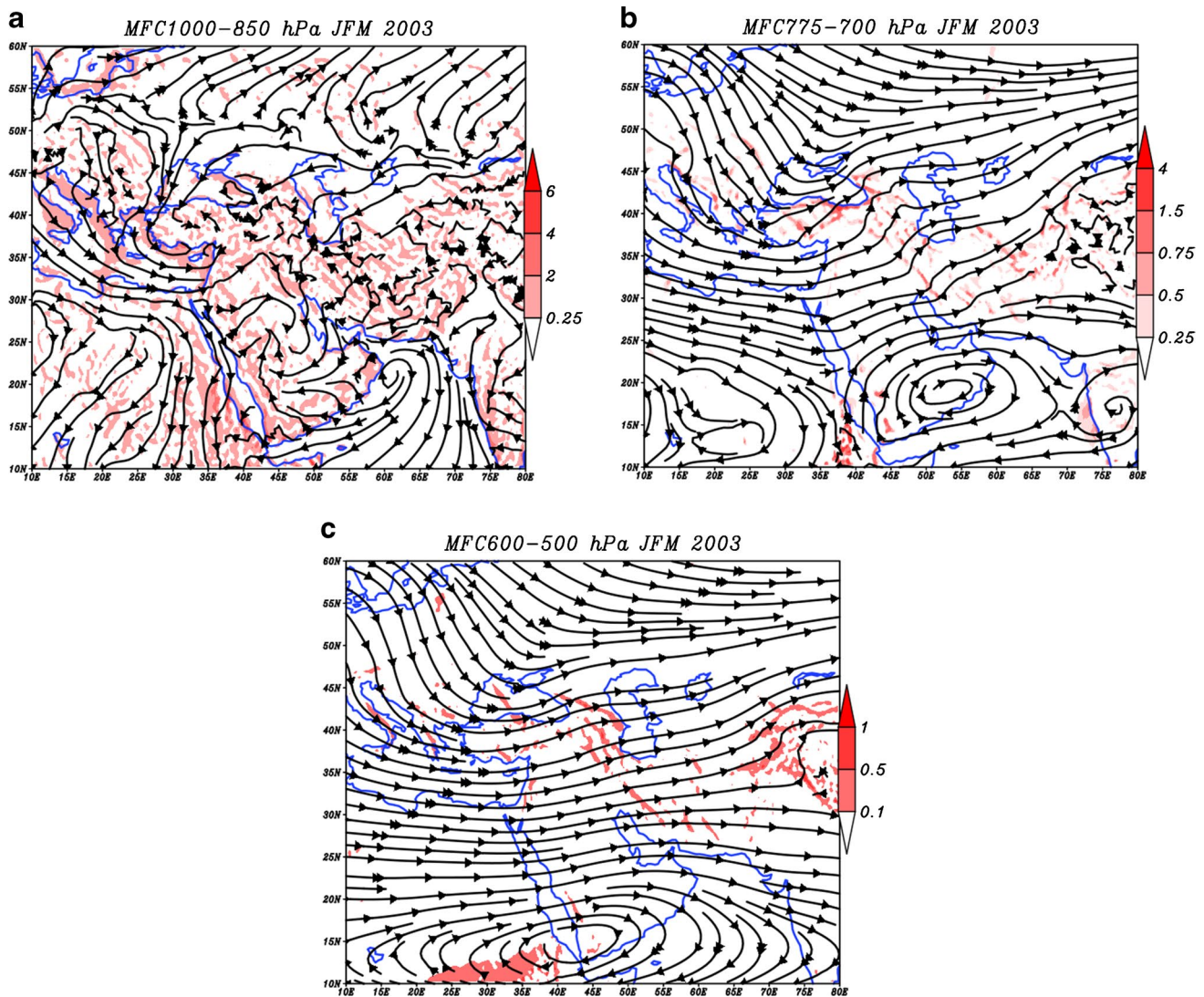
Fig. 7 **a** MFC in the lower layer (1000–850 hPa), **b** middle layer (750–700 hPa), and **c** upper layer (600–500 hPa) of the troposphere in winter 2003 (January to March)

the humidity and upward air currents in Iran. It was observed that anticyclonic currents and circulation resulting from the positive pressure anomaly from the north of Europe covers the whole country with a north to south direction. The pressure values in Iran were located in its western half, showing an increase of 1.5 hPa compared to the long term. The small size of the wind vectors was another indication of Iran's drought and atmosphere stability during winter 2003. In the middle level of the troposphere (Fig. 8b), a large field of anticyclone anomalies with anticyclonic circulation from the African continent, passing through the arid continent of the Arabian Peninsula, has covered most of Iran. Under these conditions, the Mediterranean and Sudanese cyclones, which were the most important factors in absorbing and transferring moisture to the interior of Iran, were not able to penetrate, and advection of moisture to Iran caused the conditions

for drought. The conformity of the map of the precipitation rate anomaly in mm/day (Fig. 8c) with the pressure anomaly maps at sea level and the geopotential height of the mid-level indicated the complexity of climate and the role of various factors and teleconnection indices-synoptic scales in creating negative precipitation anomaly on different parts of the Middle East, Northern Europe, and Russia.

Spring 1992

During spring 1992 in Iran (similar to winter 2003), the ENSO was in the medium El Niño phase. On the contrary, the precipitation anomaly was positive. In this regard, the synoptic condition corresponding to increasing the intensity and range of spring precipitation in the year 1992 was described at the following. According to the pressure map
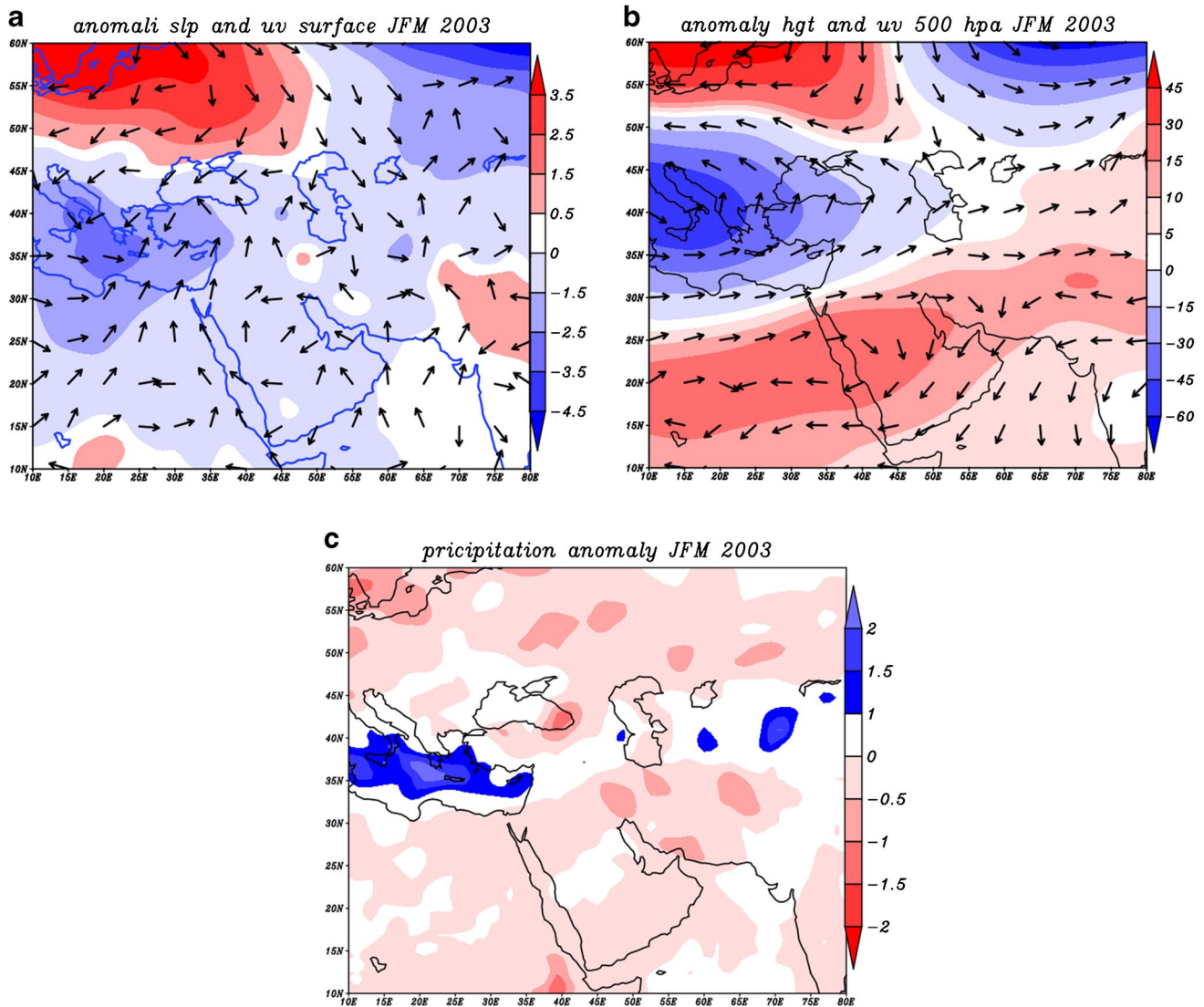
Fig. 8 **a** Sea level pressure anomaly and wind currents. **b** Geopotential height anomaly of 500 hPa. **c** Winter precipitation anomaly in the year 2003 (January to March) compared to the 30-year period (1981–2010) climatology

and wind vector of spring 1992 (Fig. 9a), the formation of multi-core low-pressure patterns in Saudi Arabia, the Persian Gulf, and east of Iran caused most of Iran's exposure to pressure values less than 1014 hPa. By weakening the cold high-pressure systems of the upper latitudes, low-pressure tongues could be able to transfer the warm and humid airs from adjacent water sources into Iran in different directions. In the geopotential height of mid-level of the troposphere of spring 1992 (Fig. 9b), unlike winter 2003, geopotential height map showed the expansion of height trough from Europe and Russia to southern Saudi Arabia, weak height ridge on Atlantic ocean, the compression and become meridian of height contours caused strengthening the divergent and upward currents in Iran. Simultaneously, with penetration of deep troughs in the Middle East, the change in the

length of Arabian sub-tropical anticyclones from zonal to meridian (southwest to northeast) makes it possible to create low-pressure systems on the Middle East.

Based on MFC maps in the three troposphere layers, it was observed that with changing the direction of wind flow, the intensity and range of positive MFC on Iran increased. In the lower layer (Fig. 10a) of the troposphere (1000–850 hPa), the central low heights, southwest, and south generally experienced the maximum humidity increasing absorption. In the lower layer of the troposphere, the circulation flow of MFC changed to the south-north, causing the humidity advection from the Arabian Sea and the Gulf of Aden into Iran. Retreat of high-pressure systems to high latitudes, the tongues resulting from multi-core low-pressures in east of Iran, the low-pressure multi-core
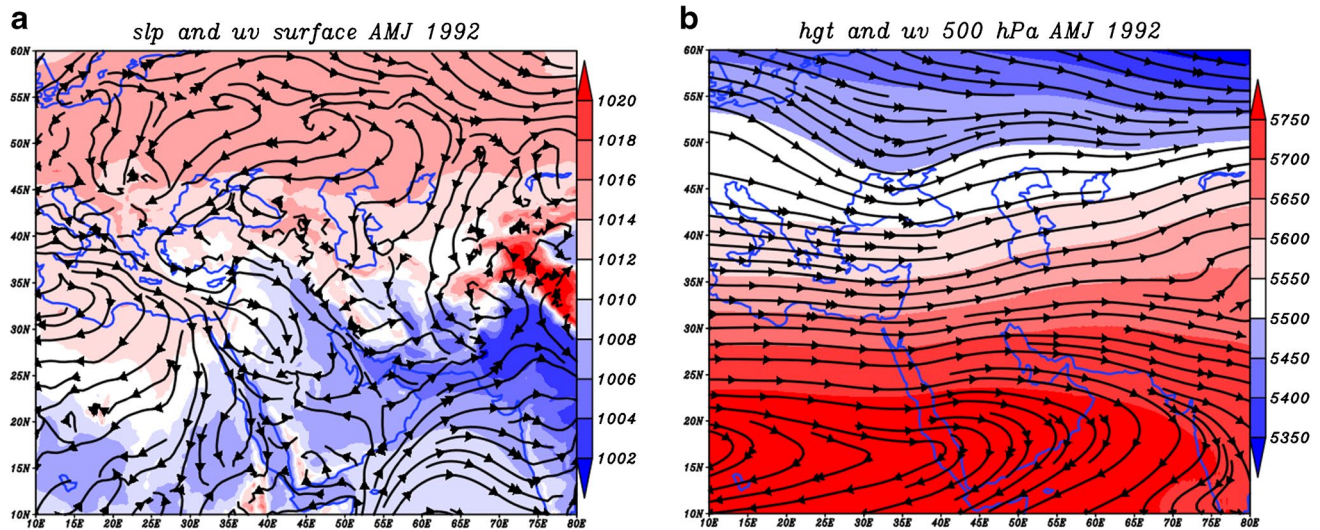
Fig. 9 a Pressure fields (color highlighted) and wind flow (contour lines) at sea level in spring 1992 (April to June). **b** Geopotential height (color) and wind flow at 500 hPa in spring 1992 (April to June)

low pressure of Iran, Saudi Arabia, and the Mediterranean with penetration in Iran converged the humidity and caused reinforcing precipitation systems. Also, in the middle and upper layers of the troposphere (Fig. 10b, c), with retreats, the Arabian sub-tropical high pressure and penetration deep trough in Iran caused intense warm and humid air divergence from adjacent water resources to the country. Therefore, the role of humidity transfer from the south was more obvious. Analysis of the MFC route showed that Saudi Arabia anticyclone was active in the middle and upper layers, and by anticyclonic movement, took the humidity of the Middle East seas from the Oman and Arabian seas and with crossing the Red Sea and the Persian Gulf (southwest-northeast direction), pumping into high pressure and re-activating the cyclone. Finally, the western systems provided the conditions for upward and the southern systems and the needed water vapor of spring 1992.

Examination of the pressure and wind vector anomaly at sea level (Fig. 11a) during spring 1992 showed that on the sea level the pressure field increased by more than 0.5 hPa compared with the long term. In the spring, unlike the winter pattern, with increasing positive pressure anomalies in the northwest of the Arabian Sea and changing the wind direction (air flow from the south and west) facilitated the conditions for penetration of large volumes of humidity of the southern seas into Iran. Along with the anomaly conditions of the surface level, like the middle layer of the atmosphere (Fig. 11b), the highest height decrease with 40 geopotential/m was located on the northern half of Iran, which covers the whole of the Mediterranean basin and the Middle East to Russia. The combination of these conditions, mean convergence movement in the sea level

with divergence and ascending and cyclonic currents in the middle layer, caused the higher discharge of humidity in the closed air and occurrence of suitable precipitation in spring and positive precipitation anomaly (Fig. 11c). A noteworthy feature in the examined anomaly maps was the role of different factors from distant regions, especially temperature and pressure changes in the Pacific and India and Atlantic oceanic regions in changing the atmospheric conditions on a synoptic and even regional scales around the world (e.g., partial changes in water temperature affect other parameters).

Conclusions

Precipitation fluctuations in each region are usually affected by different variables, and one of the most important parameters is the teleconnection indices. These indices are the indicators of feedbacks of the changes in ocean currents around the world and, as a result, affect such large-scale phenomena as planetary waves, air masses, and fronts. As noted before, these indicators are quantitative variables reflecting the behavior of the climate system; therefore, it can be said that the more intense these phenomena are, the more intense their effects on climatic variables are. Our findings showed that the seasonal and annual precipitation anomalies of Iran's sub-basins in the warm phase of ENSO (El Niño) were positive (more precipitation) and in the cold phase of ENSO (La Niña) was negative (less precipitation). In the autumn season of the El Niño phase, SBL and SKD sub-basins were positive and significant; in La Niña, WSB, KRK, and LUD sub-basins were negative and significant; and in neutral,
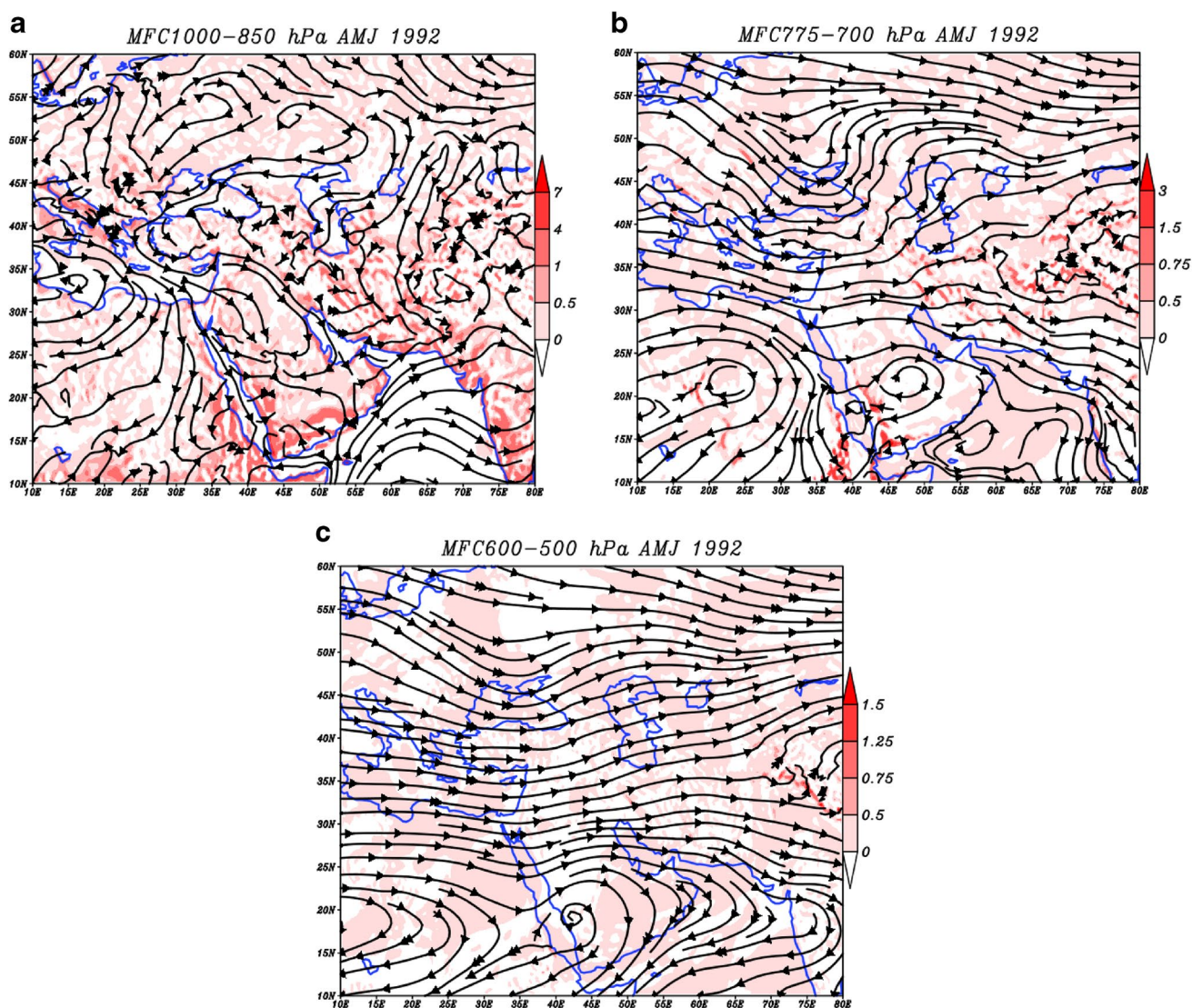
Fig. 10 **a** MFC in the lower layer (1000–850 hPa), **b** middle layer (750–700 hPa), and **c** upper layer (600–500 hPa) of troposphere on spring 1992 (April to June)

ATR, MND, LUD, CTD, DJD, KHD, and HAM sub-basins were negative and significant and SFR sub-basin were positive and significant. In the winter in the El Niño, La Niña, and neutral phases, there was no significant anomaly. In the spring, during the El Niño phase, 5 sub-basins of CS, 2 sub-basins of PG, basin of UL, and 3 sub-basins of CP and QQ basins experience the significant positive anomalies; in the La Niña phase, 5 sub-basins of CS, 2 sub-basins of PG and UL basins, and 3 sub-basin of QQ basin and CP experience negative significant precipitation anomalies; and also, in the neutral phases, any sub-basins showed the significant anomalies. The results showed that the annual precipitation anomalies of the El Niño phase would be mainly positive and significant (3 sub-basins of CS, 2 sub-basins of PG, UL basin, 2 sub-basins of CP and QQ basin) and neutral (in

1 sub-basin of CS and URL of UL are negative and positive and significant, respectively). It seems that the main cause of this lack of clear effect of ENSO in winter was the equilibrium phase of the cooling-heating of the northern hemisphere's water zones, disruption of the balance of one side of the heating–cooling atmosphere–ocean. This process was due to the inertia of the oceans' water heating capacity, causing the impact of regional compulsions such as NAO to have more weight this season than the global compulsions of ENSO. Apparently, it suggests doing more in-depth study. The final results showed the most intense of autumn precipitation anomalies occurred in the western basins in intense El Niño and La Niña and winter precipitation in the northern and western parts of Iran in strong La Niña. On the other hand, the most intense of spring precipitation anomalies
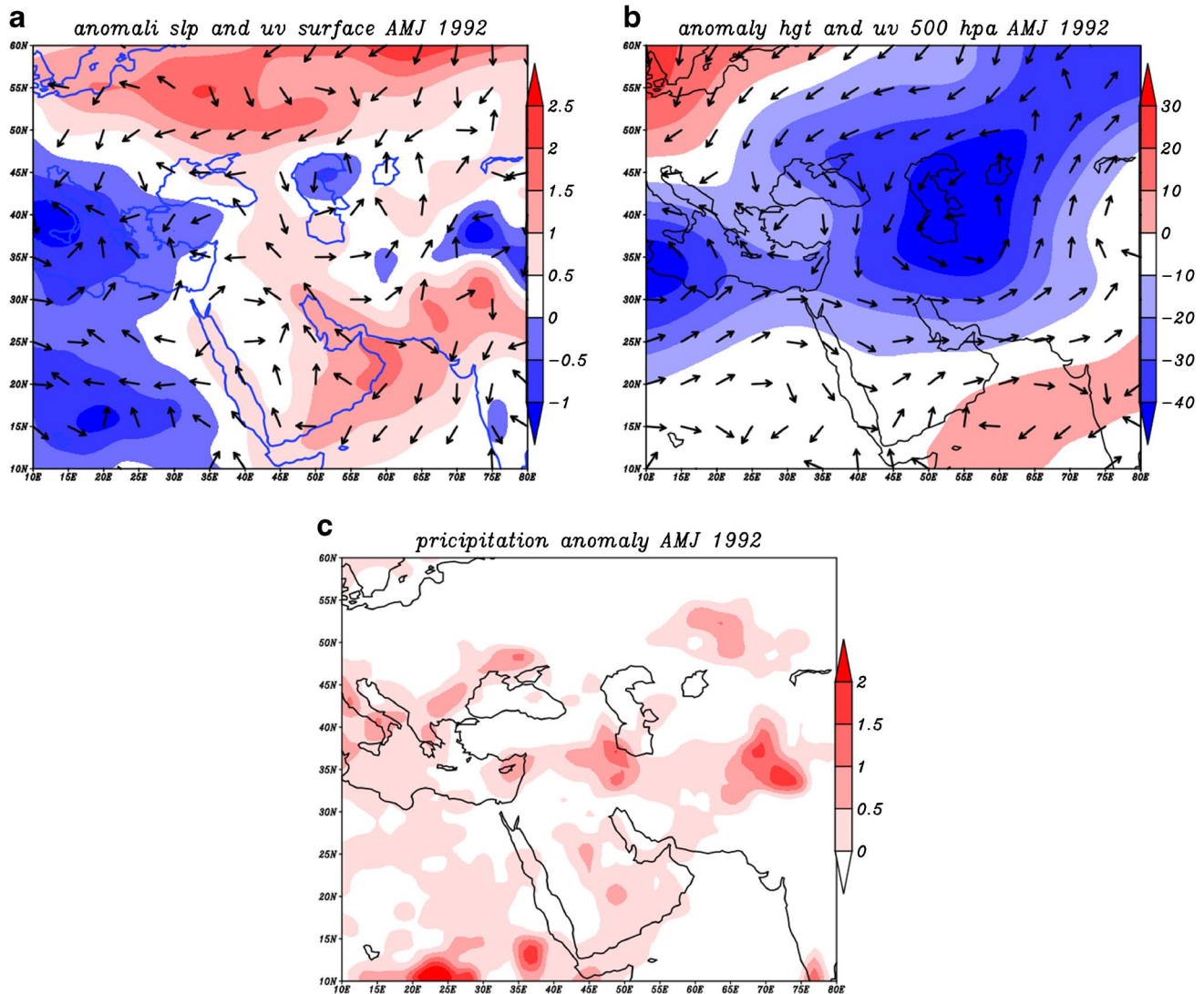
Fig. 11 **a** Sea level pressure anomaly and wind vector. **b** Geopotential height anomalies and 500 hPa wind currents. **c** Spring precipitation anomalies of 1992 (April to June) compared to 30-year (1981–2010) climatology

occurred in the northern and western parts of medium El Niño and La Niña, while the most intense of annual precipitation anomalies also took place in the El Niño and La Niña in large parts of the western, southwestern, northeastern, and southwestern. Though most of the sub-basins in central, half eastern, and southeastern plateaus were less affected by the ENSO phenomenon, the intensity of annual and seasonal precipitations anomalies in different intensities was intensified in comparison with different phases of ENSO.

Recognition the large-scale of atmospheric circulation and explaining the interactions with characteristics and specifications of regional and local scales makes it possible to understand the dominant climate system in the regions. Synoptic analysis of occurrence conditions of negative precipitation anomaly in winter 2003 and positive precipitation anomaly of spring 1992 during the El Niño

phase with the normal condition showed that during the winter with negative precipitation anomaly, the increased geopotential height over the Atlantic Ocean, strong zonal advection, persists and extended convergence from anticyclone was the most reasons of negative precipitation anomalies in winter. During spring 1992, which experienced positive precipitation anomalies, Saudi Arabia's high-pressure system retreats, and its settlement on the Oman and Arabian Seas (penetration of deep troughs on the southern latitudes) causes humidity and heat injection by Saudi Arabia to the low height's troughs of the Middle East and increasing the intensity and extension of Iran's precipitations (Darand and Pazhoh 2019a, b). In the negative anomaly of precipitation with westward movement and establishment, the anticyclone from Oman and Arabian Seas toward the Arabian Peninsula, increasing

of positive anomaly and strengthening the height ridge as integrated and with an zonal extension from the middle of the Atlantic Ocean within 10 to 30° with Crossing Africa and Iran to Center of Asia, and also along the meridian, excessive stretch of the ridge from the middle of the Atlantic and African oceans to the sub-polar regions as a blocking system, caused diverting western winds to higher latitudes and non-turbulence condition and stable atmospheric in the vast part of the Middle East and Iran. These results showed that various factors and elements affect the climate change of a region and ENSO was one of the most important indicators.

The study of precipitation anomalies in different ENSO intensities also showed an increase in intensity compared to different phases of ENSO, so that both the frequency of sub-basins with significant anomalies and also anomaly intensities increased (increasing the spatial extent of anomalies), which is different from Ahmadi Givi et al. (2010) analysis and is consistent with Rasmusson (1984) and Dehghani et al. (2020). Rasmusson (1984) shows that the strongest ENSO event increases precipitation in the southwestern of the USA, especially during the autumn season of the year that ENSO starts and also in the subsequent spring season (it is somewhat like this behavior in the west of Iran). Because in water resources studies, the long-term and short-term managements of the basin scale are preferable to the station and point scale. Dehghani et al. (2020) shown the Southern Oscillation Index (SOI), NAO, and PDO have the most impact on seasonal precipitation, respectively. Additionally, these indices have the highest impact on the precipitation in winter, autumn, spring, and summer, respectively. SOI has a diverse impact on winter precipitation compared to the PDO and NAO, while in the other seasons, each index has its special impact on seasonal precipitation. The present study analyzed the seasonal and annual precipitation anomalies in different ENSO phases and intensities at the total sub-basins of Iran and concluded that the impact of different ENSO intensities (size or absolute magnitude of ENSO) than its different phases on Iran's precipitation is more intense which it varies according to the climatic and geographical diversity of Iran in different sub-basins.

Author contribution JH and SAH: conceived the presented idea, developed the theory, and performed the computations. HM and SS: verified the analytical methods. SAH and SS: investigated and supervised the findings of this work. ML, SMM, GMM, FP, and MA: encouraged and developed the theoretical formalism. All authors discussed the results and contributed to the final manuscript.

Declarations

References

Ahmadi M, Salimi S, Hosseini SA, Poorantiyosh P, Bayat A (2019) Iran's precipitation analysis using synoptic modeling of major teleconnection forces (MTF). Dyn Atmos Oceans 85:41–56

Ahmadi Givi F, Parhizkar D, Hajjam S (2010) The study of the ENSO's effect on the seasonal precipitation of Iran in the period 1971–2000. J Earth Space 35(4):95–113

Araghi A, Martinez CJ, Adamowski J, Olesen JE (2019) Associations between large-scale climate oscillations and land surface phenology in Iran. Agric For Meteorol 278:107682

Araghinezhad SH, Shabanpour F, Jamali S (2016) Data analysis for effect of El Nino on annual rainfall in Iran. Proceeding of 6th National Congress on Water Resource Management of Iran. 1–3 May, Kourdestan University, Iran, 1–10

Atif RM, Almazroui M, Saeed S, Abid MA, Islam MN, Ismail M (2020) Extreme precipitation events over Saudi Arabia during the wet season and their associated teleconnections. Atmos Res 231:104655. https://doi.org/10.1016/j.atmosres.2019.104655

Banacos PC, Schultz DM (2005) The use of moisture flux convergence in forecasting convective initiation: historical and operational perspectives. Weather Forecast 20:351–3636

Darand M, Pazhoh F (2019a) Synoptic analysis of sea level pressure patterns and vertically integrated moisture flux convergence VIMFC during the occurrence of durable and pervasive rainfall in Iran. Dyn Atmos Ocean 86:10–17

Darand M, Pazhoh F (2019b) Vertically integrated moisture flux convergence over Iran. Clim Dyn 53:3561–3582

Dee D, Uppala SM, Simmons AJ, Berrisford P, Poli P, Kobayashi S, Andrae U, Balmaseda MA, Balsamo G, Bauer P, Bechtold P, Beljaars AC, Berg LV, Bidlot J, Bormann N, Delsol C, Dragani R, Fuentes M, Geer AJ, Haimberger L, Healy SB, Hersbach H, Holm EV, Isaksen L, Kållberg PW, Köhler M, Matricardi M, McNally AP, Monge-Sanz B, Morcrette JJ, Park B, Peubey C, Rosnay PD, Tavolato C, Thepaut J, Vitart F (2011) The ERA-Interim reanalysis: configuration and performance of the data assimilation system. Q J R Meteorol Soc 137:553–597

Dehghani M, Salehi S, Mosavi A, Nabipour N, Shamshirband S, Ghamisi P (2020) Spatial analysis of seasonal precipitation over Iran: co-variation with climate indices. ISPRS Int J Geo Inf 9(2):73. https://doi.org/10.3390/ijgi9020073

Ghaedamini H, Nazemosadat SMJ, Kouhizadeh M, Sabziparvar AA (2014) Individual and coupled effects of the ENSO and PDO on autumnal dry and wet periods in the southern parts of Iran. Iran J Geophys 8(2):92–109

Ghasemi AR, Khalili D (2008) The association between regional and global atmospheric patterns and winter precipitation in Iran. Atmos Res 88:116–133

Ghodousi H, Kooshafar L (2018) Simultaneous use of climatic signals and sea surface temperature for flow forecasting (case study: Cheshmeh Kileh catchment area). Iran J Soil Water Res 49(5):1044–1053

Gong DY, Wang SW (1999) Impacts of ENSO on global precipitation changes and precipitation in China. Chin Sci Bull 44(9):852–857

Grimm AM, Ferraz SET, Gomes J (1998) Precipitation anomalies in southern Brazil associated with El Nino and La Nina events. J Clim 11:2863–2880

HashemiDovin M (2013) Evaluation of multivariate El Nino Index (MEI) effect on North Khorasan winter precipitation. J Clim Res 13:31–44

Helali J, Salimi S, Lotfi M, Hosseini SA, Bayat A, Ahmadi M, Naderizarneh S (2020) Investigation of the effect of large-scale atmospheric signals at different time lags on the autumn precipitation of Iran's watersheds. Arab J Geosci 13(18):1–24

Helali J, Momenzadeh H, Oskouei EA, Lotfi M, Hosseini SA (2021a) Trend and ENSO-based analysis of last spring frost and chilling in Iran. Meteorol Atmos Phys. https://doi.org/10.1007/s00703-021-00804-2

Helali J, Hosseinzahef T, Cheraghalizadeh M, MohammadiGhalenei M (2021b) Feasibility study of using climate teleconnection indices in prediction of spring precipitation in Iran Basins. Iran J Soil Water Res 52(3):749–769

Jiang R, Wang Y, Xie J, Zhao Y, Li F, Wang X (2019) Assessment of extreme precipitation events and their teleconnections to El Niño Southern Oscillation, a case study in the Wei River Basin of China. Atmos Res 218:372–384

Kadioğlu M, Tulunay Y, Borhan Y (1999) Variability of Turkish precipitation compared to El Niño events. Geophys Res Lett 26:1597–1600

Kahya E, Dracup JA (1994) The influences of type 1 El Niño and La Niña events on stream flows in the Pacific southwest of the United States. J Clim 7:965–976

Kalimeris A, Ranieri E, Founda D, Norrant C (2017) Variability modes of precipitation along a Central Mediterranean area and their relations with ENSO, NAO, and other climatic patterns, Atmospheric Research: 56–80.

Khorshiddoust AM, GhavidelRahimi Y (2006) The evaluation of the effect of ENSO feature on variability of seasonal precipitation in eastern Azerbaijan province using multivariate ENSO index (MEI). Geogr Res Q 38:15–26

Liesch T, Wunsch A (2019) Aquifer responses to long-term climatic periodicities. J Hydrol 572:226–242

MohammadiSabet V, Mousavi Baygi M, Rezaee Pazhand H (2017) Comparative study of the effects of ENSO phenomenon (El Niño, La Niña) on temperature and precipitation of Mashhad. J Water Soil 30(6):2101–2114

Mohammadrezaei M, Soltani S, Modarres R (2020) Evaluating the effect of ocean-atmospheric indices on drought in Iran. Theor Appl Climatol. https://doi.org/10.1007/s00704-019-03058-6

Monzon JP, Sadras VO, Andrade FH (2012) Modelled yield and water use efficiency of maize in response to crop management and Southern Oscillation Index in a soil-climate transect in Argentina. Field Crop Res 130:8–18

Nalley D, Adamowski J, Biswas A, Gharabaghi B, Hu W (2019) A multiscale and multivariate analysis of precipitation and streamflow variability in relation to ENSO, NAO and PDO. J Hydrol 574:288–307

Nazemosadat MJ, Cordery I (2000) On the relationships between ENSO and autumn rainfall in Iran. Int J Climatol 20(1):47–61

Nazemosadat MJ, Ghasemi AR (2004) Quantifying the ENSO-related shifts in the intensity and probability of drought and wet periods in Iran. J Clim 17(20):4005–4018

Nicholson SE (2001) The relationship between El-Nino and drought. J Clim 14:323–335

Pagano TC, Mahani SH, Nazemosadat MJ, Sorooshian S (2003) Review of Middle Eastern hydroclimatology and seasonal teleconnections. Iran J Sci Technol 27(B1):95–109

Price C, Stone L, Huppert A, Rajagopalan B, Alpert P (1998) A possible link between El Niño and precipitation in Israel. Geophys Res Lett 25:3963–3966

Rahimi D, Abdollahi K, Hasheminasab S (2016) Identify tele-connection patterns affecting on rainfall in Karoon Basin. Iran J Echohydrol 3(1):95–105

Rasmusson EM (1984) El Nino, the ocean atmosphere connection. Oceanus 27:5–12

Rasmusson EM, Wallace JM (1983) Meteorological aspects of the El Niño/southern oscillation. Science 222:1195–1202

Sabziparvar A, Firoozmand Z, Varshavian V (2020) The impact of teleconnection phenomena on shifting the date of first autumn and last spring frost events. Phys Geogr Res Q 52(2):295–331

Ropelewski CF, Halpert MS (1986) North American precipitation and temperature patterns associated with El-Niño-Southern Oscillation (ENSO). Mon Weather Rev 114:2165–2352

Schmidt N, Lipp EK, Rose JB, Luther ME (2001) ENSO influences on seasonal rainfall and river discharge in Florida. J Clim 14(4):615

Tabari H, TalaeeHosseinzadeh P (2011) Temporal variability of precipitation over Iran: 1966–2005. J Hydrol 396:313–320

Wang G, Hendon HH (2007) Sensitivity of Australian rainfall to inter-El Nino variations. J Clim 20:4211–4226

Zanchettin D, Franks SE, Traverso P, Tomasino M (2008) On ENSO impacts on European wintertime rainfalls and their modulation by the NAO and the Pacific multi-decadal variability described through the PDO index. Int J Climatol 28(8):995–1006

Authors and Affiliations

Jalil Helali[1] · Hossein Momenzadeh[2] · Saadoun Salimi[3] · Seyed Asaad Hosseini[4] · Mohammad Lotfi[2] · Seyedeh Maryam Mohamadi[5] · Gholamreza Maghami Moghim[6] · Farshad Pazhoh[3] · Mohammad Ahmadi[7]

Jalil Helali
jalilhelali@gmail.com

Hossein Momenzadeh
h.momenzadeh@srbiau.ac.ir

Saadoun Salimi
Saadun1989@gmail.com

Mohammad Lotfi
lotfim48@yahoo.com

Seyedeh Maryam Mohamadi
Maryam_mohamadi110@yahoo.com

Gholamreza Maghami Moghim
maghami_dr@yahoo.com

Farshad Pazhoh
farshad.pazhooh44@gmail.com

Mohammad Ahmadi
moahmadi04@gmail.com

[1] Department of Irrigation and Reclamation Engineering, Faculty of Agricultural Engineering and Technology, University of Tehran, Karaj, Iran

[2] Department of Earth Sciences, Science and Research Branch, Islamic Azad University, Tehran, Iran

[3] Department of Climatology, Kharazmi University, Tehran, Iran

[4] Department of Physical Geography (Climatology), Mohaqheqh Ardabili University, Ardabil, Iran

[5] Department of Environment Monitoring Expert, Tehran, Iran

[6] Department of Geology Science, University of Damghan, Semnan, Iran

[7] Kermanshah Regional Meteorological Office, Kermanshah, Iran